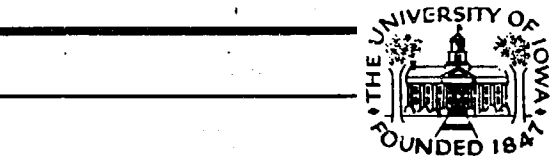




"Original contains color plates: All DTIC reproductions will be in black and white"

Department of Physics and Astronomy
THE UNIVERSITY OF IOWA
Iowa City, Iowa 52242

U. of Iowa 89-21

# Diagnosis of Auroral Dynamics Using Global Auroral Imaging with Emphasis on Large-Scale Evolutions

by

J. D. Craven and L. A. Frank

September 1989

Department of Physics and Astronomy

The University of Iowa

Iowa City, Iowa 52242-1479



"Original contains color plates: All DTIC reproductions will be in black and white"

To be published in Auroral Physics,
ed. by C.-I. Meng, M. J. Rycroft and L. A. Frank,
Cambridge University Press, Cambridge (England), 1989

SECURITY CLASSIFICATION OF THIS PAGE

# REPORT DOCUMENTATION PAGE

Form Approved OMB No. 0704-0188

| | |
|---|---|
| 1a REPORT SECURITY CLASSIFICATION: Unclassified | 1b RESTRICTIVE MARKINGS: None |
| 2a SECURITY CLASSIFICATION AUTHORITY: --- | 3 DISTRIBUTION / AVAILABILITY OF REPORT: Unlimited, cleared for public release and sale |
| 2b DECLASSIFICATION / DOWNGRADING SCHEDULE: --- | |
| 4 PERFORMING ORGANIZATION REPORT NUMBER(S): U. of Iowa 89-21 | 5 MONITORING ORGANIZATION REPORT NUMBER(S): |
| 6a NAME OF PERFORMING ORGANIZATION: The University of Iowa; 6b OFFICE SYMBOL (If applicable): | 7a NAME OF MONITORING ORGANIZATION: Office of Naval Research |
| 6c ADDRESS (City, State, and ZIP Code): Department of Physics and Astronomy, Iowa City, IA 52242-1479 | 7b ADDRESS (City, State, and ZIP Code): Univ. of Washington, 315 Univ. District Bldg., 1107 NE 45th St, Seattle, WA 98105-4631 |
| 8a NAME OF FUNDING / SPONSORING ORGANIZATION: Office of Naval Research; 8b OFFICE SYMBOL (If applicable): | 9 PROCUREMENT INSTRUMENT IDENTIFICATION NUMBER: N00014-85-K-0404 |
| 8c ADDRESS (City, State, and ZIP Code): 800 N. Quincy Street, Arlington, VA 22217-5000 | 10 SOURCE OF FUNDING NUMBERS: PROGRAM ELEMENT NO; PROJECT NO; TASK NO; WORK UNIT ACCESSION NO |

11 TITLE (Include Security Classification): Diagnosis of Auroral Dynamics Using Global Auroral Imaging with Emphasis on Large-Scale Evolutions

12 PERSONAL AUTHOR(S): Craven, John D. and Frank, Louis A.

| 13a TYPE OF REPORT | 13b TIME COVERED | 14 DATE OF REPORT (Year, Month, Day) | 15 PAGE COUNT |
|---|---|---|---|
| Journal Article | FROM _____ TO _____ | September 1989 | 60 |

16 SUPPLEMENTARY NOTATION: ---

| 17 COSATI CODES | | | 18 SUBJECT TERMS (Continue on reverse if necessary and identify by block number) |
|---|---|---|---|
| FIELD | GROUP | SUB-GROUP | Aurora<br>Geomagnetic storms, substorms |
| | | | |
| | | | |

19 ABSTRACT (Continue on reverse if necessary and identify by block number)

See page following.

| | |
|---|---|
| 20 DISTRIBUTION / AVAILABILITY OF ABSTRACT: ☐ UNCLASSIFIED/UNLIMITED ☒ SAME AS RPT ☐ DTIC USERS | 21 ABSTRACT SECURITY CLASSIFICATION: Unclassified |
| 22a NAME OF RESPONSIBLE INDIVIDUAL: Bob Silverman | 22b TELEPHONE (Include Area Code): 206/543-2656; 22c OFFICE SYMBOL: |

DD Form 1473, JUN 86 — Previous editions are obsolete. — SECURITY CLASSIFICATION OF THIS PAGE

## ABSTRACT

The spatial extent of the auroral oval and polar cap for typical auroral conditions covers an area of about 20 $Mkm^2$, for which a minimum of more than 20 well-placed ground stations is required for full spatial coverage, even if significant difficulties such as sunlight, moonlight, geography, and meteorology are neglected. As shown here, auroral imaging with high-altitude spacecraft provides substantial advantages relative to ground-based techniques. Variations in the dimensions of the auroral oval with changes in the sign of the Z component of the interplanetary magnetic field (IMF) are easily observed. Auroral luminosities all along the auroral oval increase within minutes following arrival at the magnetosphere of a shock in the interplanetary medium. It appears that the dawn-dusk motion of the large-scale transpolar arc of a theta aurora observed in the northern (southern) polar cap is in the same (opposite) direction as the $B_y$ component of the IMF. It is shown that the onsets of auroral substorms occur within a range of less than 3.5 hours of magnetic local time centered at 2250 MLT. This is nearly identical to the statistically determined location for the initial response to substorm onset at the orbits of geosynchronous spacecraft. The auroral bulge does not always expand symmetrically in the east-west direction from the position of substorm onset, but can progress preferentially into either the evening or morning sector.

# 1. INTRODUCTION

Ground-based auroral scientists are hampered in their investigations of the aurora by viewing limitations imposed by geography, meteorology and season. Observations are made at night in the high-latitude, polar regions (hence a preference for the winter season), in the absence of significant cloud cover. In addition, the desire for minimum interference by moonlight can preclude observations near full moon. A single observer can view an area of about 2 $Mkm^2$ at 120-km altitude when provided with an unobstructed view of the horizon above an elevation angle of $5^o$. This area is small in comparison to the 21-$Mkm^2$ area of the auroral zone and polar cap at magnetic latitudes $>67^o$. Hence more than 10 well-placed ground-based observing sites are required to carry out a 24-hours/day observation program within the polar cap and auroral oval in the dark hemisphere. More than 20 observing sites are required for a more reasonable minimum elevation angle of $10^o$.

While a campaign to uniformly monitor the polar region has never been attempted, large and well-organized campaigns have taken place in which numerous ground-based sites were distributed at polar latitudes. The International Geophysical Year (IGY) of 1957-1958 [Annals of the IGY] is an outstanding example of such an effort at the international level. Auroral observations acquired during the IGY are responsible for the significant increase in our knowledge of the spatial distribution of the aurora during the early 1960s, including the description of the continuous distribution of emissions encircling the magnetic pole, i.e., the auroral oval [see Feldstein and Galperin, 1985, and references therein], and the formulation of the first global-scale description of auroral dynamical behavior, the auroral substorm [Akasofu, 1963, 1964].

With the advent of orbital ob ving platforms during the IGY it was quickly recognized that images from space would provide the next important step in

investigations of the global distributions of aurora. Success in achieving that next step is seen in the auroral images from the spacecraft ISIS 2 [Anger et al., 1973; Shepherd et al., 1973], DMSP [Rogers et al., 1974], KYOKKO [Kaneda, 1979], Dynamics Explorer [Frank et al., 1981], HILAT [Meng and Huffman, 1984], Viking [Anger et al., 1987] and Polar BEAR [Meng et al., 1987]. A brief summary of the principal wavelengths, relevant orbital parameters, and resolutions of these imagers is provided by Frank and Craven [1988].

Here, various aspects of the large-scale spatial distribution of the aurora and its dynamic evolution as viewed from space are discussed. We concentrate on results from auroral images gained at high altitudes with the spacecraft Dynamics Explorer 1 [Hoffman et al., 1981], for which the spacecraft apogee altitude is 3.65 earth radii ($R_e$), and the orbital inclination and period are $90^o$ and 6.83 hours, respectively. The DE-1 auroral imaging instrumentation comprises three imaging photometers, two for observations at visible wavelengths and one at vacuum-ultraviolet (VUV) wavelengths. Effective full angle of an individual pixel is $0.29^o$, which provides a linear dimension for a pixel of 32 km per $R_e$ of spacecraft altitude. Hence the images generally provide a spatial resolution of the order of a hundred kilometers. Images to be discussed here, at VUV wavelengths, are acquired with filter passbands for which the principal auroral emission features are (1) the $N_2$ Lyman-Birge-Hopfield (LBH) bands, (2) $N_2$ (LBH) and the OI multiplets at about 130.4 and 135.6 nm, and (3) the same as (2) with the addition of a background of geocoronal Lyman-α radiation. These filters are referred to herein at 1, 2 and 3, respectively, where the number designates the increasing passband of the filter. A detailed discussion of the instrumentation is provided by Frank et al. [1981].

The observations discussed here are presented in four sections, beginning in the next section with a summary of the basic global-scale dimensions of the

auroral distribution and the variations in auroral activity with the north-south orientation of the interplanetary magnetic field (IMF). A discussion of the theta aurora, which represents the large-scale limit of sun-aligned arcs in the polar cap during periods of northward-directed IMF, follows. The global auroral response to the arrival at Earth of shocks in the interplanetary medium is outlined in the fourth section, using examples for northward and southward IMF. Finally, there is an overview of large-scale auroral features observed during auroral substorms, which are of greatest importance during periods of southward IMF.

## 2. LARGE-SCALE SPATIAL DISTRIBUTIONS

The large-scale spatial distributions of the aurora at polar latitudes in the two terrestrial hemispheres are readily illustrated with the DE-1 auroral images of Figures 1 and 2. These false-color images of the aurora borealis (Figure 1) and the aurora australis (Figure 2), with overlays of the coastlines, show that, when not distinguishing between discrete and diffuse forms, the aurora can form a continuous ring of optical emissions encircling each magnetic pole. The south magnetic pole (for which the vector direction of the field is toward the pole) is located near the northwest coast of northern Greenland (Figure 1) and the north magnetic pole is positioned near the sunward side of the gap in optical emissions along the transpolar arc (Figure 2). In each case, the high-latitude boundary of the instantaneous auroral oval in magnetic coordinates is nearly represented by a circle [see Meng et al., 1977]. For this northern view in Figure 1 during active auroral conditions, the latitudes of the poleward boundary are about $73^{\circ}$ and $74^{\circ}$, respectively, at local noon and midnight, nearly centered on the magnetic pole. The boundary is shifted by several degrees toward the morning sector. For the southern view of Figure 2, with a northward IMF, the poleward boundaries are located at about $80^{\circ}$ and $70^{\circ}$, which yields a $5^{\circ}$ antisunward offset nearly symmetric in the dawn-dusk plane. This antisunward offset of about $5^{\circ}$ is in good agreement with the statistically derived shape of the poleward boundary as reported by Meng et al. [1977].

Diameters of the auroral ovals as presented here are approximately equal to the longitudinal width of Canada (5200 km) and to the cross section of the Antartic continent (4800 km). The areas of circles of these diameters are 21 and 18 $Mkm^2$, respectively. Measurement of the actual areas encircled by the high- and low-latitude boundaries of the aurora are 12.7 and 24.2 $Mkm^2$, respectively, for the aurora of Figure 1, and 9.1 and 19.0 $Mkm^2$ for the aurora of Figure 2.

These are representative values. Hudson Bay in eastern Canada provides a convenient geological length scale for determining fields-of-views for ground-based observers, as its maximum longitudinal width of about 1000 km is equivalent to the distance at 120-km altitude that a ground-based observer views for elevation angles >10.5°. The area of a 1000-km diameter circle is 0.79 $Mkm^2$, or about 1/25th of the area of the instantaneous oval and polar cap. Additional specific examples of the useful field-of-view for a ground-based observer are provided in Figure 2 of Frank and Craven [1988] and Craven et al. [1989a].

While the large-scale spatial distribution of these emissions is continuous, distinct local time variations seen in the images are not continuous along the entire auroral oval. In Figure 1, for example, localized, more discrete auroral forms are present in the midnight sector at the high latitude boundary, while more uniform (diffuse) emissions at lower latitudes extend towards the local noon sector from midnight. Localized features are also noted in the early afternoon hours, where for this image in the northern hemisphere local time advances in the counterclockwise direction. In the conjugate hemisphere (Figure 2) localized, bright emissions are again seen in the early afternoon hours, where in the southern hemisphere local time advances in the clockwise direction. These localized enhancements in the early afternoon hours of local time are probably associated with enhanced electron precipitation and its effects observed at those local times [Evans, 1985, and references therein]. The transpolar arc which bisects the southern auroral oval will be discussed in the next section.

The auroral distribution is not always continuous across the local noon sector, but can display a prominent midday gap [e.g., Meng, 1981a, and references therein]. In particular the discrete auroral arcs can appear to be absent in the noon sector. A clear example of this midday gap in the discrete aurora is shown in Figure 3, for an observation of the northern auroral oval on 8 December 1981

from an altitude of 1.92 $R_e$. The emissions are from the $N_2$ (LBH) bands. Three arcs are visible in the evening sector along the lower portion of the image, with the brightest arc at lowest latitude extending westward to a local [illegible]320 MLT. A surge is visible at 1920 MLT, in the lower-right portion of [illegible]s emissions in the late-morning sector do not extend past 0925 MLT, [illegible]t gap extends over 4 hours of local time. Auroral brightnesses within the gap are at, or near, the photometer sensitivity threshold of 300 R, and the latitudinal widths of the discrete auroral forms in the evening sector are seen at the limiting spatial resolution of the photometer. This gap is readily detected here in the absence of bright diffuse emissions at lower latitudes, which are present in the images of Figures 1 and 2.

The auroral images presented in Figures 1 and 2 represent two typical, but not simultaneous, views of the aurora in the two hemispheres. Simultaneous views of the aurora in the two hemispheres with a single spacecraft can only be obtained if the spacecraft is located at high altitudes and low latitudes. A view of the northern auroral oval from near the equator has been presented earlier by Frank and Craven [1988] during a brief period of spacecraft eclipse early in the DE mission. Several imaging sequences in this same several-week period of spacecraft eclipses in February 1982 have also provided simultaneous images of the two auroral ovals through a fortuitous combination of Universal Time and spacecraft position. The example presented in Figure 4, with coastal outlines and limb of the solid Earth overlaid on the image, is a particularly outstanding example of such simultaneous imaging from a single spacecraft. The plane of the $90^o$ inclination orbit bisects the image vertically, and acts to highlight the offset of the magnetic dipole axis aligned about $11^o$ clockwise in this image obtained at 1215 UT on 1 March 1982.

The large-scale spatial distribution of auroral emissions varies with time in response to the north-south orientation of the IMF [e.g., Akasofu, 1977]. To demonstrate this, consider in Figure 5 variations in the IMF $B_Z$ component and the auroral electrojet index AE for the 54-hour time interval beginning at 0000 UT on 24 October 1981 (day 297). The IMF is monitored with magnetometers onboard the ISEE-3 spacecraft near the $L_1$ libration point about 235 $R_e$ upstream in the solar wind [data courtesy of E. J. Smith], and with ISEE 1 in earth orbit [data courtesy of C. T Russell]. The correction of 50 min for the transit time of magnetic signatures in the IMF from ISEE 3 to ISEE 1 has been made by comparing limited simultaneous observations from the two spacecraft. While the acquisition of telemetry is not continuous throughout the time interval, sufficient coverage is provided to establish the overall pattern of variations in the north-south orientation. The field is oriented northward during the first six hours, and then becomes more nearly aligned in the X-Y plane (geocentric solar magnetospheric coordinates) until about 1000 UT on the same day. The field then turns and remains southward for the next 30 hours. It returns to a northward orientation after 1600 UT on 25 October (day 298).

The response of the auroral electrojet as measured by the AE index during this day is also shown in Figure 5 and is typical for the observed variations in the orientation of the IMF. During the intervals of northward IMF at the beginning and end of the 54-hour time interval, the magnitude of the index is much less that 100 nT and does not vary significantly. The first large, impulsive increase in AE to 200 nT just after 0600 UT on 24 October is preceded by the decrease in magnitude of $B_Z$ to approximately 0 nT. The large increase in AE to 1000 nT is closely associated with the decrease in $B_Z$ to -10 nT. Enhanced activity along the auroral electrojet continues for more than 25 hours. The nearly monotonic

increase in $B_Z$ after 1200 UT on 25 October is accompanied by a concomitant decrease in electrojet activity.

It is not possible in a limited space to provide the full collection of auroral images obtained in the eight orbits of DE 1 during a little more than the 54-hour interval. A compact summary is provided in Figure 6 by selecting one image from each consecutive orbit, where the position along the orbit is nearly identical as possible for each image. Below each image is given the year, day of year and time (UT) of acquisition. Unfortunately, the same filter is not used for each of the nine orbits, but the filters, emission lines, and other supporting information are summarized in Table 1. The first image (1) is located at upper left in the figure, and time advances from left-to-right and top-to-bottom. The last image (9) is at the lower right. The image times are identified in Figure 5 by numbered black bars across the center of the figure.

A weak transpolar arc is visible in the first image (filter 2, 2333 UT, 23 October) of Figure 6, consistent with the earlier northward orientation of the IMF (not shown) [Frank et al., 1986]. Auroral brightnesses are reduced significantly for the second image with filter 1 for $N_2$(LBH) emissions only. Fortuitously, the time for this image corresponds to the first sharp increase in AE and reveals the onset near midnight of a small, localized and brief auroral substorm shortly after the southward turning. The next five images (3 through 7) capture the auroral oval during ongoing auroral activity typical for periods of southward IMF and initial recovery from an extended period of southward orientation. The third image (filter 3, 1326 UT, 24 October) presents the first observation of a substorm expansion phase which began less than 12 min earlier. Particular attention should be given to this substorm onset, because the AE index (Figure 5) decreases rapidly with the onset and then recovers by about 1345 UT to values of 600-700 nT observed just prior to this onset. This sharp decrease in AE with the onset of

substorm activity is not an isolated example, and can be found in observations at oth[illegible]es. This further demonstrates that care must be exercised when using the AE index for the identification of individual substorms. It is presumed, but not yet demonstrated, that such decreases are associated with particular spatial distributions of ground magnetometers and the auroral electrojet during some substorms.

The next four images are obtained during the expansion or recovery phases of distinct substorms, as follows: image 4, late expansion; images 5 and 6 late expansion or early recovery; image 7, late recovery. Discrete auroral forms are faintly observed along the poleward boundary of the auroral in the evening-to-midnight sectors in each of these four examples. The last two images (8 and 9) reveal again, for northward IMF orientations, a less dynamic auroral oval similar to that observed in the first two images. Identical filters are used for images 1 and 8 (filter 2) and for images 2 and 9 (filter 1), as summarized in Table 1. The threshold luminosity was established at about 2 kR at image processing for images 3-7, and was lowered to about 1 kR for the weaker auroral luminosities of images 1, 2, 8 and 9.

## 3. MOTION OF THE THETA AURORA

An early perception of the polar cap in auroral research was that of a dark, relatively unimportant region poleward of the classical discrete aurora which was devoid of interesting auroral phenomena. This view has evolved with careful observations and with improving sensor sensitivities, and now it is recognized that the polar cap aurora represents the optical signature of important plasma processes within the magnetotail-ionosphere system which are most prominent when the IMF is directed northward. Physical details of these processes and an understanding of the mapping to the distant magnetotail are less well developed than those of the diffuse and discrete aurora along the auroral oval, as plasma sources are more readily identifiable in terms of the plasma sheet and the plasma sheet boundary layer.

Sun-aligned arcs were first studied extensively with ground-based instrumentation [e.g., Lassen and Danielson, 1978, and references therein]. As summarized by Lassen and Danielsen from such observations, the arcs are prominent when the IMF is northward and are observed throughout the polar cap, with a greater occurrence in the morning sector. Low-altitude DMSP spacecraft images have also been used to determine the spatial distribution of sun-aligned polar cap arcs. For three classifications of arcs observed for quiet magnetic conditions and northward IMF, Gussenhoven [1982] has shown that the sign of the IMF $B_y$ component is important in classifying the spatial distributions. Gussenhoven concludes that the arcs occur most frequently in the morning sector (P(2) classification) for $B_y < 0$ and in the evening sector (P(3)) for $B_y > 0$, with arcs near the center of the polar cap (P(1)) associated with small values of $B_y$. Again, arcs are observed most frequently in the morning sector, but this is due to the fact that for these observations $B_y$ is negative more frequently than it is positive. A similar investigation by Ismail and Meng [1982], with DMSP auroral

images, identifies three types of polar cap sun-aligned arcs: type 1, distinct arcs within the central polar cap; type 2, arcs near the evening and morning sectors of the auroral oval; and type 3, arcs near local midnight which realign along the auroral oval towards the evening sector or towards both the evening and morning sector. The type-1 and -3 arcs are observed infrequently, i.e., 4% and 0.4% occurrence frequencies, respectively. The type-2 arcs are observed more frequently in the morning sector. Ismail and Meng [1982] associate the type-2 arcs with an expansion of the auroral oval to higher latitudes. Arc lengths can exceed 1000 km. Correlations with IMF orientation yield greatest occurrence frequencies for northward-directed fields, and the type-1 arcs are observed more frequently in the northern (southern) hemisphere when $B_X$ is negative (positive). It is important to recall that most DMSP auroral images do not provide a view of the entire polar cap.

With the launch of DE 1 in late 1981 global auroral imaging at 6-to-12 minute temporal resolution became available with imaging sequences of up to 5 hours duration. Early in the analysis program large-scale auroral forms of several hundreds of kilometers width were observed within the polar cap to extend continuously from the midnight to the noon sector across the polar cap [Frank et al., 1982]. There are no reports in the previous literature of the existence of large-scale transpolar arcs such as that shown in Figure 2. These unique auroral forms are observed to move in directions generally perpendicular to the Sun-Earth line; for a negative IMF $B_y$ component the motion in the northern hemisphere is in the dawn direction [Frank et al., 1985]. A second example of motion in the northern polar cap, but with positive $B_y$ has recently been discussed by Huang et al. [1989]. The position of the transpolar arc on 25 March 1982 at 0538 UT is shown in the single image at left in Figure 7, with the selected section within the rectangle enlarged at right. As a summary of the arc motion throughout the

interval of observations (0514-0757 UT), the location of the arc approximately midway between the two intersections with the auroral oval has been mapped magnetically into the magnetotail using the model field of Tsyganenko and Usmanov [1982] for Kp > 3+, and the $Y_{gsm}$ position of the arc at $X_{gsm}$=-12 $R_e$ is shown in Figure 8. Note that for $B_y > 0$ the motion is towards the dusk sector. The average speed is 6.6 km/s. In contrast, at southern polar latitudes a single outstanding sequence of observations associated with the image of Figure 2 demonstrates that for positive $B_y$ the transpolar arc can move in the dawn direction, opposite to that in the northern hemisphere. This is demonstrated in Figure 9 with the same magnetic mapping technique. The average speed of the arc is 8.9 km/s.

Simultaneous measurements of a single bright arc in the two polar caps with low-altitude, polar-orbiting spacecraft are difficult due to the trajectories of the spacecraft relative to the diurnally displaced auroral oval and the offset magnetic dipole. Nevertheless, such observations may have been accomplished by Gorney et al. [1986] for a bright arc observed in the northern hemisphere with DMSP-F6 and NOAA-7 plasma instruments and in DMSP-F6 images, and in the southern hemisphere with the NOAA-6 plasma instrument. An arc is observed in the morning sector in both hemispheres, separated from the auroral oval. However, it is not determined from the observations if the arc is a transpolar arc. It is unclear how to interpret this observation in light of (1) the DE-1 observations which suggest that transpolar arcs move in opposite directions (hence one would not expect the northern and southern arcs, if the same feature in two polar caps, to both be in the morning sector) and (2) the DMSP observations of Ismail and Meng [1982], which suggest that the $B_x$ component may select a preferred hemisphere. One suggestion is that the arc observed by Gorney et al. really is a type-2 arc as identified by Ismail and Meng [1982] at the poleward boundary of the

auroral oval at high latitudes [see Meng, 1981b]. Observations similar to those of Gorney et al. are reported by Obara et al. [1988] from Viking auroral images in the northern hemisphere and EXOS-C observations of precipitating electrons in the southern polar cap. The Viking images show clearly the presence of a transpolar arc in the morning sector of local time. Obara et al. conclude that an arc is also present in the morning sector of the southern polar cap.

If polar cap arcs map magnetically into the plasma sheet [Frank et al., 1982, 1986; Peterson and Shelley, 1984], then it is expected that plasma signatures similar to those observed within the plasma sheet and its boundary layer will be intercepted with spacecraft normally within the lobes of the magnetotail. Such plasma signatures for structures aligned along the Z-X plane are reported by Huang et al. [1987]. In contrast to the results of Gorney et al. and Obara et al., Huang et al. [1989] report that observations of a transpolar arc in the evening sector of the northern polar cap appear to be accompanied by plasma structures in the morning sector of the southern lobe. Simultaneous optical observations of transpolar arcs in the northern and southern polar caps with Viking and DE 1, respectively, on 3 August 1986 [Craven et al., 1989b] provide the clearest evidence to date for a dawn-dusk asymmetry in the position of transpolar arcs and their motion in opposite directions.

At the limit of weak (subvisual) 630-nm optical emissions, the principal observations continue to be made from the ground. It is concluded that these Sun-aligned arcs within the polar caps arise from sheet-like distributions of precipitating low-energy (hundreds of electron volts) electrons that maintain current continuity at shears in the plasma flow across the polar cap during magnetically quiet periods [Reiff et al., 1978; Carlson et al., 1984]. The Sun-aligned arcs drift in the dawn-dusk plane while the dominant plasma flow direction is in the antisunward direction. Within the velocity shear the flow can

be reduced in magnitude, stagnant or sunward [Carlson et al., 1984]. Simultaneous ground-based observations within two 1000-km diameter fields-of-view demonstrate that these weak, Sun-aligned arcs can extend across a significant fraction of the polar cap, and that they represent "the dominant optical character of the northward IMF polar cap" [Carlson, 1988, and as presented at the 1988 Spring AGU Meeting].

In brief review, it appears clear that Sun-aligned arcs represent the dominant discrete auroral feature of the polar cap for magnetic quiet periods of positive $B_Z$, and are present over a wide range of brightnesses and wavelengths associated with variations in characteristic energies of precipitating electrons along velocity shears in the plasma flows. There is no reason to expect different physical processes at the extremes of arc brightness and physical dimensions. Least frequently observed of the Sun-aligned arcs is the large-scale transpolar arc. It is reasonable to associate this feature with the P(1) classification of Gussenhoven [1982] and with the type-3 aurora of Ismail and Meng [1982]. The transpolar arcs move generally transverse to the Sun-Earth line, with the direction of motion controlled by the sign of the IMF $B_Y$ component.

## 4. RESPONSE TO SHOCKS IN THE INTERPLANETARY MEDIUM

A shock in the interplanetary medium arriving at Earth applies a compressive force which reduces the overall dimensions of the near-Earth magnetospheric cavity and must alter the magnitudes and distributions of currents and plasmas around and within the cavity. One well-established signature of changes in the locations and magnitudes of these currents is an increase in the horizontal component of the magnetic field detected with magnetometers at low-latitude ground stations. The surface field at all local times begins to increase abruptly, in <1 min, in response to the compression [e.g., Nishida, 1978]. Of greater significance for the magnetosphere is the subsequent onset of a geomagnetic storm, in which the terrestrial ring current undergoes a rapid enhancement in a matter of hours, the low-latitude magnetic field decreases by hundreds of nanoteslas, and auroral activity increases dramatically a higher latitudes [e.g., Akasofu, 1977, and references therein]. For such cases, a preceding sudden increase in the low-latitude magnetic field accompanying the magnetospheric compression is labeled the storm sudden commencement (SC), and the subsequent rapid decrease in the magnetic field is called the main phase of the storm.

There is also an immediate magnetospheric response to the arrival of an interplanetary shock in the form of enhanced energetic (tens of kiloelectron volts) electron precipitation along the auroral oval. These increases are observed with riometers and balloon-borne x-ray detectors [e.g., Brown et al., 1961; Matsushita, 1961; Ortner et al., 1962; Ullaland et al., 1970]. Within the magnetosphere a significant increase is noted in the probability of observing energetic particle bursts in the magnetotail and magnetosheath [Tholen and Armstrong, 1986]. Increases in auroral luminosities are also reported [Vorob'yev, 1974; Craven et al., 1986]. The enhancement can begin simultaneously (<1 min) with SC onset and last

for 3-10 min [Vorob'yev, 1974] or longer [Craven et al., 1986]. The magnitude of the enhancement varies from about 10% to factors of >2, depending on the method of detection, and also varies from event to event. The immediate increase in auroral luminosities is not associated with onset of an auroral substorm. The auroral electrojet is also observed to respond to a shock arrival (see the brief summary by Craven et. al., [1986], and references therein).

The case study of two moderate geomagnetic substorms by Craven et al. [1986] with auroral images from DE 1 illustrates the immediate large-scale influence on the aurora following the arrival at Earth of a shock in the interplanetary medium. Magnetic activity for geomagnetic storms on 20 and 22 October 1981 is summarized in Figure 10, where the $D_{st}$ and $K_p$ indices are plotted, respectively, in the upper and lower panels. Sudden commencements are detected at 1309 UT on 20 October and at 0525 UT on 22 October. The orientation of the IMF is southward before the first SC and during the main phase decrease in $D_{st}$. In contrast, it is northward for the second event. The main phase onset following the second SC is delayed for more than two hours until the IMF turns southward. It is only then that significant auroral activity begins, as noted coarsely with the three-hour $K_p$ index in the lower part of Figure 10 or with the AE index (not shown). The AE indices and IMF data for these events are given by Craven et al. [1986]. The importance of the southward turning of the IMF for the initiation of the main phase of a geomagnetic storm has been shown by Akasofu [1977, Figure 5.18].

The auroral response to the magnetospheric compression on 22 October 1981 can be seen in the 12-image sequence of Figure 11. The false-color format is again used in which weaker luminosities of several kilorayleighs (kR) are coded in red and the greater luminosities of the active aurora and from the sunlit hemisphere (about 20 kR) are coded orange to yellow. For these observations the

ultraviolet photometer operates in a mode for which an image is obtained with filter 3 and the next image is acquired with filter 2. The two-filter sequence repeats cyclically. The first image, at 0417 UT, is with filter 3, which passes Lyman-α radiation. The weak emissions observed above Earth's limb in the first image of Figure 11 are due to scattering of solar Lyman-α radiation by exospheric hydrogen [e.g., Rairden et al., 1986]. The filter passband for the second image, at 0429 UT, excludes responses due to the Lyman-α radiation.

The IMF orientation prior to and during the shock crossing is northward. The first five images of this sequence (0417 to 0525 UT) are taken prior to arrival of the shock. Auroral luminosities around the oval increase noticeably in the sixth image at 0525 UT, and remain enhanced for the duration of the imaging sequence. As shown in Figure 12b (from the work of Craven et al. [1986]), auroral luminosities increase from about 2 kR before the shock crossing to 6-8 kR within 10 min after the crossing. The increases in luminosities after the shock crossing are observed more clearly for northward IMF due to the generally lower luminosities along the auroral oval during the period prior to the crossing. An example of this can be seen in Figure 12a for a shock crossing at 1309 UT on 20 October in the presence of a southward IMF. Note that the luminosities are about 4-6 kR prior to the shock crossing. The imaging sequence for this event is provided in the work of Craven et al. [1986].

The last four images of Figure 11 demonstrate that the aurora brightens at midnight about 30-min after the shock crossing and a Sun-aligned polar arc begins to form at midnight. The Sun-aligned polar arc then lengthens across the polar cap to local noon at an average speed of 1 km/s. This sunward expansion of the arc is similar in speed to westward traveling surges, which move along pre-existing arcs in the late-evening sector. Faint Sun-aligned auroral forms undetected with DE 1 may have been present within the polar cap in advance of

the shock impact as part of the established polar cap convection pattern. No significant increases are observed in the magnitude of the AE index during this period of arc formation.

For the single example discussed here in some detail, and for the companion case with southward IMF also discussed in detail by Craven et al. [1986], the onset of significant auroral activity about 30 min after shock impact is independent of the sign of $B_Z$ and may be related to a time constant for reconfiguration of the geomagnetic tail in response to changes in the interplanetary medium behind the shock.

## 5. AURORAL SUBSTORMS

The concept of the auroral substorm as first described by Akasofu [1964] provides a general description of a particular class of large-scale dynamical variations observed along the auroral oval. In this description, an auroral substorm begins near local magnetic midnight as a rapid, localized brightening along previously quiet arcs and proceeds with disruption of the ordered distribution of the arcs. A significant point is that the onset begins along an arc, and not within the diffuse auroral emissions equatorward of the arcs. Second, the onset need not occur along the most equatorward arc, though it usually does. The disruption of the longitudinally extended, stable arcs into patches and arc fragments at substorm onset is known as the auroral breakup. The region of enhanced auroral luminosities and rapidly moving auroral forms, the auroral bulge, expands quickly in longitude along the arcs, and less rapidly to higher latitudes. Diffuse emissions appear at lower latitudes. Surge activity at the westward edge of the auroral bulge can expand rapidly westward [e.g., Akasofu et al., 1965, 1966c; Craven et al., 1989a], with average speeds of apparent westward expansion ranging from several hundred to several thousand meters per second. The classical westward traveling surge apparently is not due to the westward motion over thousands of kilometers of a single surge, but is due to the sequential formation of a series of relatively localized surges at progressively greater distances westward along the auroral oval [e.g., Tighe and Rostoker, 1981; Craven et al., 1989a]. The westward expansion of the auroral bulge is also observed on occasion to cease abruptly early in the expansion phase and to remain nearly stationary for much of the expansion phase [e.g., Rostoker et al., 1987; Craven and Frank, 1987; Craven et al., 1989a]. Eastward expansion of the breakup is also highly variable, and can also expand well into the morning sector [e.g., Craven and Frank, 1987] or can stop abruptly early in the expansion phase [Shepherd et al.,

1987]. The range of speeds for the poleward expansion is similar to that for westward traveling surges [see Akasofu et al., 1965, 1966a], and the speed varies with time and local time in the expansion phase [e.g., Craven and Frank, 1987]. The expansion generally develops through the ongoing formation of new arcs at progressively higher latitudes [e.g., Davis and Kimball, 1960; Kisabeth and Rostoker, 1974]. The formation of new arcs does not appear to occur at a uniform rate, but occurs episodically at intervals of 10-15 min [e.g., Kisabeth and Rostoker, 1974; Craven and Frank, 1987]. These individual, more-rapid poleward advances are believed to be associated with the individual substorm intensifications, or multiple substorm onsets. Equatorward of the most poleward arcs within the auroral bulge, auroral forms are observed to move equatorward [e.g., Snyder and Akasofu, 1972]. Equatorward expansion of the aurora takes place at rates of tens to several hundreds of meters per second [see Akasofu et al., 1966b; Craven and Frank, 1987], and has been observed in some instances to exceed the rate of poleward expansion [Snyder and Akasofu, 1972]. The duration of the expansion phase of the substorm is highly variable, from tens of minutes to hours, and is terminated with the absence of additional new arcs at higher latitudes. The end of this expansion phase is followed by a recovery phase, in which the auroral luminosities diminish, the poleward and equatorward expansions become contractions, and longitudinally extended quiet arcs begin to reform. The duration of a typical substorm cycle is 2 - 3 hours. Additional specific details of auroral morphology are given by Akasofu [1977] and references therein.

The physical location of substorm onset is difficult to identify from the ground due to the several considerations discussed previously. Low-altitude spacecraft such as DMSP are hampered significantly by the low sample rate of a single image per polar transit, usually about 100 min for the same hemisphere. High-altitude continuous imaging provided by DE 1 and Viking is not so restricted.

A survey in search of images of auroral substorm onsets has been made using DE observations for the time interval from 24 September 1981 through 10 February 1982. It is important to limit the survey to those images for which the auroral bulge is still of limited spatial extent (in order to reduce the error in determining the location of onset), and for which subsequent images demonstrate the continuing development of a substorm. The first image of Figure 13 represents a good example of the localized onset, and a second example is provided by Frank and Craven [1988, in Figure 12]. Neither of these examples is from the original survey. From the initial survey, a total of 68 onsets have been identified which meet the two selection criteria. For each event, the geographic coordinates of onset have been measured and the corrected geomagnetic local time and latitude have been computed. The local time distribution for these onsets is shown in Figure 14 without restriction on the magnetic latitude of onset, which varies from $59^{o}$ - $72^{o}$. The median value is $65^{o}$. The mean and median values of MLT for the histogram are the same and are 2250 MLT (22.8 hours). The width of the distribution is 3.5 hours for more than two samples per half-hour interval. The average latitudinal width of the auroral bulge for the 68 cases is $1.1^{o}$. These observations confirm the well-known but not well-documented fact that auroral substorm onsets are observed most frequently late in the premidnight sector.

An investigation of substorm-related plasma injections and magnetic field reconfigurations at geosynchronous altitudes by Arnoldy and Moore [1983] finds that the initial signature of a substorm at the geosynchronous altitude occurs within a limited region of local time centered just before midnight (see Figure 7 of Arnoldy and Moore [1983]). Their analysis shows that the time delay between arrival of substorm-related changes at the two spacecraft is dependent on the local times of the spacecraft: to the west (east) of the onset the more easterly

GOES 2 (westerly GOES 3) observes the effect first. The spacecraft positions are separated by two hours in local time. At a particular pair of local times for the two spacecraft the time delay is zero and it is presumed that the two spacecraft are located symmetrically in longitude about the local time of onset. Using a simple unweighted least-squares fit of median values in one-hour increments of local time, the data of their Figure 7 yields a local time of 2300 MLT for zero time delay. This local time is nearly identical to the 2250 MLT obtained above for the DE observations, thereby confirming that statistically there is a close spatial relation in local time between auroral substorm onset and the onset of a reconfiguration of current systems within the inner magnetosphere at geosynchronous altitudes.

The large-scale latitudinal and longitudinal motions of the aurora in the southern hemisphere for the particularly active period following the onset at about 0202 UT on 13 June 1983 are also shown in Figure 13. The expansion phase continues until about 0410 UT (eleventh image). The development of the terrestrial ring current and the auroral electrojet for this active period are summarized with the $D_{st}$ and AE indices, which are plotted, respectively, in Figure 15 and the lower panel of Figure 16. This imaging sequence follows a SC at 0118 UT and occurs during a main phase decrease in a geomagnetic storm and development of an enhanced terrestrial ring current. The intense, brief increase in the luminosities at all local times at 0327 UT (eighth image of Figure 13) is what would be expected following a shock crossing, as discussed in the previous section, thereby suggesting an encounter with a second shock or discontinuity in the interplanetary medium. Accompanying this large-scale enhancement in the luminosities at 0327 UT is a significant, localized perturbation of the auroral oval to lower latitudes near 0540 MLT, (the eighth and ninth images of Figure 13), suggesting a large-scale perturbation in the outer magnetosphere in the dawn

sector. (Local time advances in the clockwise direction for these images of the southern hemisphere.) The perturbation extends equatorward by about 4° from the 63° magnetic latitude of the auroral oval in the previous images. Also, a significant localized enhancement in luminosities is seen in the early afternoon sector at 1350 MLT, beginning with the eighth image [see Evans, 1985, and references therein]. Luminosities along the auroral oval decline to earlier values after the tenth image.

The latitudinal motions of the aurora during this substorm are presented in Figure 16, with motions at 2000, 2200 and 2400 MLT shown in the upper panel and at 0000, 0200 and 0400 MLT in the center panel. The measurements at midnight are reproduced in each panel to facilitate comparisons. The several significant points are (1) the poleward expansion is reasonably symmetric along the eight hours of local time at an average speed of 375 m/s, (2) the equatorward expansion is asymmetric, with an average speed of about 97m/s near midnight, and decreases slightly in the morning sector, (3) the recovery phase at high latitudes begins after 0410 UT with no indication of a "poleward leap" [Hones, 1985] separating the expansion and recovery phases, (4) the poleward boundary during the recovery phase is complex, with the beginning time for the recovery phase varying with local time [e.g., Snyder and Akasofu, 1972; Kisabeth and Rostoker, 1974; Craven and Frank, 1987], (5) the AE index remains at large values of the order of 1600 nT well into the recovery phase, and (6) the recovery at the equatorward boundary begins in the premidnight sector at about 0440 UT, but is not detected in the postmidnight sector by the end of the imaging sequence at 0517 UT. Not resolved in this sequence at 12-min temporal resolution are the episodic poleward expansions observed in less intense substorms [e.g., Craven and Frank, 1987].

The symmetric poleward expansion displayed for this interval of intense auroral activity is not a consistent feature of substorms. To demonstrate this, the spatial distribution of aurora is shown in Figure 17 for a selected image during the expansion phase of each of four substorms. The first image, at 1549 UT, is from a sequence of images on 4 November 1981 for which a substorm onset is identified at about 1525 UT. The greater luminosities of a surge near the western edge of the auroral bulge identify the approximate local time of the onset. The westward edge of the bulge did not advance along the auroral oval during this substorm. The second image at 1123 UT on 7 April 1983 follows a substorm onset at about 1023 UT. The onset occurred near local midnight and the expanding auroral bulge is more nearly symmetric about midnight. The third image at 1849 UT on 30 March 1983 is nearly a mirror image of the first image, with the eastern edge of the auroral bulge remaining nearly stationary, and the auroral bulge expanding into the evening sector. Substorm onset is after 1825 UT. The last image, from a study by Craven et al. [1989a], shows that a very small substorm near local midnight can be accompanied by an intense, westward traveling surge. The presence of a westward traveling surge is verified by simultaneous ground observations, and the DE-1 images show that the auroral bulge at local midnight is small. The four images show that poleward expansion of the auroral bulge need not be symmetric about midnight or the location of onset, but can be highly asymmetric. The four images presented in Figure 17 are selected to demonstrate also that asymmetries are observed in both hemispheres. The first and fourth (second and third) images of the figure were obtained in the northern (southern) hemisphere. The images are all displayed with the dusk sector to the left. It is not yet known if the orientation of the IMF influences the asymmetric development of the bulge or how the asymmetry in one hemisphere maps to the

conjugate hemisphere. Simultaneous imaging in the two hemispheres is required, as is provided by DE 1 and Viking.

Schematic illustrations are provided in Figure 18 to assist in outlining these local time variations. For each of the four examples, in magnetic coordinates, the initial spatial distribution of auroral arcs is denoted by a single, global-scale quiet auroral arc. Recall that the high-latitude boundary of the auroral oval in geographic coordinates maps to a circle in magnetic coordinates [Meng et al., 1977]. Poleward and westward expansions of the auroral bulge are identified by a series of curves representing arcs. No attempt has been made to illustrate the instantaneous rates of expansion. For clarity, the magnitudes of the motions may be exaggerated from appropriate typical values, but the maximum amplitudes are not unrealistic for some extremely intense substorm expansions. Equatorward expansions are not included in these illustrations.

With these limitations in mind, an example for a minimum in westward expansion is illustrated in Figure 18a. In the midnight sector the high latitude boundary advances poleward in discrete steps as new arcs develop rapidly at higher latitudes with substorm intensifications. Repetitive intensifications of the electrojet are observed near the westward edge of the bulge, but "the surge may grow and decay in confined longitudinal sector without suffering any significant displacement" [Tighe and Rostoker, 1981]. There is no reason to preclude even more exaggerated examples of eastward expansions.

The observations of Craven et al. [1989a] are schematically illustrated in Figure 18d, for which the prominent feature is a latitudinally confined expansion of surges along the oval. Examples of westward expansions intermediate between the more extreme cases of Figures 18a and 18d are provided in Figures 18b and 18c. A surge would be observed along the auroral oval at the intersection of the pre-existing arcs of the quiet oval and the westward edge of the expanding auroral

bulge. A ground-based observer at 1800 MLT would observe a surge only if the symmetric expansion of Figure 18b proceeded sufficiently far poleward. An expansion which did not extend as far poleward at midnight would also be observed at 1800 MLT if the westward motion were more prominent (Figure 18c). Repetitive intensifications and poleward advances of the high-latitude boundary of the aurora near local midnight at intervals of 10-15 min [e.g., Craven et al., 1987, 1989a] are similar to the observed rates of intensifications and advances for surges as the westward edge of the bulge [Wiens and Rostoker, 1975]. This similarity in repetition rates further supports the inference that the poleward advance of the aurora and intensifications of the surges are directly related [see also Rostoker et al., 1987].

The physical mechanism which controls the east-west asymmetry in a substorm expansion is not known, but the orientation of the IMF deserves attention as a variable of significance. Also, variations in the orientation of the IMF prior to and/or during a substorm could lead to variations in the temporal development of the substorm. As pointed out by N. C. Maynard [private communication, 1988], the asymmetries in our Figure 18 suggest similarities to plasma convection patterns for the polar latitudes as determined by Heppner and Maynard [1987], which are dependent on the orientation of the IMF.

## ACKNOWLEDGMENTS

Magnetic field data from the ISEE-1 and -3 spacecraft were kindly provided, respectively, by C. T. Russell and E. J. Smith. This research was supported in part by NASA under grants NAG5-483 and NGL-167-001-002, and by ONR under grant N00014-85-K-0404.

Table 1

Principal Auroral Emission Features for Images of Figure 6

| Image | Day | UT | Filter | Emissions |
|---|---|---|---|---|
| 1 | 296 | 2333 | 2 | $N_2$(LBH) + OI |
| 2 | 297 | 0627 | 1 | $N_2$(LBH) |
| 3 | 297 | 1326 | 3 | $N_2$(LBH) + OI + H (Lyman α) |
| 4 | 29 | 1954 | 2 | $N_2$(LBH) + OI |
| 5 | 298 | 0305 | 3 | $N_2$(LBH) + OI + H (Lyman α) |
| 6 | 298 | 092 | 2 | $N_2$(LBH) + OI |
| 7 | 298 | 1639 | 3 | $N_2$(LBH) + OI + H (Lyman α) |
| 8 | 298 | 2341 | 2 | $N_2$(LBH) + OI |
| 9 | 299 | 061 | 1 | $N_2$(LBH) |

## REFERENCES

Akasofu, S.-I., The dynamical morphology of the aurora polaris, J. Geophys. Res., 68, 1667-1673, 1963.

Akasofu, S.-I., The development of the auroral substorm, Planet. Space Sci., 12, 273-282, 1964.

Akasofu, S.-I., Physics of Magnetospheric Substorms, D. Reidel, Dordrecht, Netherlands, 1977.

Akasofu, S.-I., D. S. Kimball and C.-I. Meng, The dynamics of the aurora - II, westward traveling surges, J. Atmos. Terr. Phys., 27, 173-187, 1965.

Akasofu, S.-I., D. S. Kimball and C.-I. Meng, Dynamics of the aurora-V, poleward motions, J. Atmos. Terr. Phys., 28, 497-503, 1966a.

Akasofu, S.-I., D. S. Kimball and C. -I. Meng, Dynamics of the aurora - VII, equatorward motions and the multiplicity of auroral arcs, J. Atmos. Terr. Phys., 28, 627-635, 1966b.

Akasofu, S.-I., C.-I. Meng and D. S. Kimball, Dynamics of the aurora - IV, polar magnetic substorms and westward traveling surges, J. Atmos. Terr. Phys., 28, 489-496, 1966c.

Anger, C. D., T. Fancott, J. McNally, and H. S. Kerr, ISIS-II scanning auroral photometer, Appl. Opt., 12, 1753-1766, 1973.

Anger, C. D., S. K. Bakey, A. L. Broadfoot, R. G. Brown, L. L. Cogger, R. Gattinger, J. W. Haslett, R. A. King, D. J. McEwen, J. S. Murphree, E. H. Richardson, B. R. Sandel, K. Smith and A. V. Jones, An ultraviolet auroral imager for the Viking spacecraft, Geophys. Res. Lett., 14, 387-390, 1987.

Annals of the International Geophysical Year, Vol. 1-47, 1959-1969, Pergamon Press, New York.

Arnoldy, R. L., and T. E. Moore, Longitudinal structure of substorm injections at synchronous orbit, J. Geophys. Res., 88, 6213-6220, 1983.

Brown, R. R., T. R. Hartz, B. Landmark, H. Leinbach and J. Ortner, Large-scale electron bombardment of the atmosphere at the sudden commencement of a geomagnetic storm. J. Geophys. Res., 66, 1035-1041, 1961.

Carlson, H. C., Jr., Polar cap sun aligned arcs (abstract), Eos Trans. AGU, 69, 440, 1988.

Carlson, H. C., Jr., V. B. Wickwar, E. J. Weber, J. Buchau, J. G. Moore and W. Whiting, Plasma characteristics of polar cap F-layer arcs, Geophys. Res. Lett., 11, 895-898, 1984.

Craven, J. D., L. A. Frank, C. T. Russell, E. J. Smith and R. P. Lepping, Global auroral responses to magnetospheric compressions by shocks in the solar wind: two case studies, in Solar Wind-Magnetosphere Coupling ed. by Y. Kamide and J. Slavin, Terra Publishing Co., Tokyo, 1986.

Craven, J. D., and L. A. Frank, Latitudinal motions of the aurora during substorms, J. Geophys. Res., 92, 4565-4573, 1987.

Craven, J. D., L. A. Frank and S.-I. Akasofu, Propagation of a westward traveling surge and the development of persistent auroral features, J. Geophys. Res., 94, 5961-6967, 1989a.

Craven, J. D., L. A. Frank, J. S. Murphree and L. L. Coggar, Simultaneous optical observations of transpolar arcs in the two polar caps with DE 1 and Viking, (abstract), Eos Trans. AGU, 70, 428, 1989b.

Davis, T. N., and D. S. Kimball, Incidence of auroras and their north-south motions in the northern auroral zone, Geophys. Inst. Rep. UAG-R100, Univ. of Alaska, Fairbanks, 1960.

Evans, D. S., The characteristics of a persistent auroral arc at high latitudes in the 1400 MLT sector, in The Polar Cusp, ed. by J. A. Holtet and A. Egeland, D. Reidel, Boston, 1985.

Feldstein, Y. I., and Yu. I. Galperin, The auroral luminosity structure in the high-latitude upper atmosphere: its dynamics and relationship to the large-scale structure of the earth's magnetosphere, Rev. of Geophys., 23, 217-275, 1985.

Frank, L. A., J. D. Craven, K. L. Ackerson, M. R. English, R. H. Eather and R. L. Carovillano, Global auroral imaging instrumentation for the Dynamics Explorer mission, Sp. Sci. Instr., 5, 369-393, 1981.

Frank, L. A., J. D. Craven, J. L. Burch and J. D. Winningham, Polar views of the earth's aurora with Dynamics Explorer, Geophys. Res. Lett., 9, 1001-1004, 1982.

Frank, L. A., J. D. Craven and R. L. Rairden, Images of the earth's aurora and geocorona from the Dynamics Explorer mission, Adv. Space Res., 5, 53-68, 1985.

Frank, L. A., J. D. Craven, D. A. Gurnett, S. D. Shawhan, D. R. Weimer, J. L. Burch, J. D. Winningham, C. R. Chappell, J. H. Waite, R. A. Heelis, N. C. Maynard, M. Sugiura, W. K. Peterson and E. G. Shelley, The theta aurora, J. Geophys. Res., 91, 3177-3224, 1986.

Frank, L. A., and J. D. Craven, Imaging results from Dynamics Explorer, Rev. Geophys., 26, 249-283, 1988.

Gorney, D. J., D. S. Evans, M. S. Gussenhoven and P. F. Mizera, A multiple-satellite observation of the high-latitude auroral activity on January 11, 1983, J. Geophys. Res., 91, 339-346, 1986.

Gussenhoven, M. S., Extremely high latitude auroras, J. Geophys. Res., 87, 2401-2412, 1982.

Heppner, J. P., and N. C. Maynard, Empherical high-latitude electric field models, J. Geophys. Res., 92, 4467-4489, 1987.

Hoffman, R. A., G. D. Hogan and R. C. Maehl, Dynamics Explorer spacecraft and ground operations system, Sp. Sci. Instr., 5, 349-367, 1981.

Hones, E. W., Jr., The poleward leap of the auroral electrojet as seen in auroral images, J. Geophys. Res., 90, 5333-5337, 1985.

Huang, C. Y., L. A. Frank, W. K. Peterson, D. J. Williams, W. Lennartsson, D. G. Mitchell, R. C. Elphic and C. T. Russell, Filamentary structures in the magnetotail lobes, J. Geophys. Res., 92, 2349-2363, 1987.

Huang, C. Y., J. D. Craven and L. A. Frank, Simultaneous observations of a theta aurora and associated magnetotail plasmas, J. Geophys. Res., 94, 10,137-10,143, 1989.

Ismail, S., and C.-I. Meng, A classification of polar cap auroral arcs, Planet. Space Sci., 30, 319-330, 1982.

Kaneda, E., Auroral TV observation by KYOKKO, Proceedings of the International Workshop on Selected Topics of Magnetospheric Physics, Japanese IMS Committee, Tokyo, 1979.

Kisabeth, J. L., and G. Rostoker, The expansive phase of magnetospheric substorms, 1. Development of the auroral electrojets and auroral arc configuration during a substorm, J. Geophys. Res., 79, 972-984, 1974.

Lassen, K., and C. Danielsen, Quiet time pattern of auroral arcs for different directions of the interplanetary magnetic field in the Y-Z plane, J. Geophys. Res., 83, 5277-5284, 1978.

Matsushita, S., Increase of ionization associated with geomagnetic sudden commencements, J. Geophys. Res., 66, 3958-3961, 1961.

Meng, C.-I., R. H. Holzworth and S.-I. Akasofu, Auroral circle-delineating the poleward boundary of the quiet auroral belt, J. Geophys. Res., 82, 164-172, 1977.

Meng, C.-I., Electron precipitation in the midday auroral oval, J. Geophys. Res., 86, 2149-2174, 1981a.

Meng, C.-I., Polar cap arcs and the plasma sheet, Geophys. Res. Lett., 8, 273-276, 1981b.

Meng, C.-I., and R. E. Huffman, Ultraviolet imaging from space of the aurora under full sunlight, Geophys. Res. Lett., 11, 315-318, 1984.

Meng, C.-I., R. E. Huffman, F. Del Greco and R. Eastes, UV images of the dayside auroral oval (abstract), Eos Trans. AGU, 68, 396, 1987.

Nishida, A., Geomagnetic Diagnosis of the Magnetosphere, Springer-Verlag, New York, 1978.

Obara, T., M. Kitayama, T. Muki, N. Kaya, S. Murphree and L. L. Cogger, Simultaneous observations of sun-aligned polar cap arcs in both hemispheres by EXOS-C and Viking, Geophys. Res. Lett., 15, 713-716, 1988.

Ortner, J., B. Hultqvist, R. R. Brown, T. R. Hartz, O. Holt, B. Landmark, J. L. Hook and H. Leinbach, Cosmic noise absorption accompanying geomagnetic storm sudden commencements, J. Geophys. Res., 67, 4169-4186, 1962.

Peterson, W. K., and E. G. Shelley, Origin of the plasma in a cross-polar cap auroral feature (theta aurora), J. Geophys. Res., 89, 6729-6736, 1984.

Rairden, R. L., L. A. Frank and J. D. Craven, Geocoronal imaging with Dynamics Explorer, J. Geophys. Res., 91, 13,613-13,630, 1986.

Reiff, P. H., J. L. Burch and R. A. Heelis, Dayside auroral arcs and convection, Geophys. Res. Lett., 5, 391-394, 1978.

Rogers, E. H., D. F. Nelson and R. C. Savage, Auroral photography from a satellite, Science, 183, 951, 1974.

Rostoker, G., A. V. Jones, R. L. Gattinger, C. D. Anger and J. S. Murphree, The development of the substorm expansive phase: the "eye" of the storm, Geophys. Res. Lett., 14, 399-402, 1987.

Shepherd, G. G., T. Fancott, J. McNally and H. S. Kerr, ISIS-II atomic oxygen red line photometer, Appl. Opt., 12, 1767-1774, 1973.

Shepherd, G. G., C. D. Anger, J. S. Murphree, and A. V. Jones, Auroral intensifications in the evening sector observed by the Viking ultraviolet imager, Geophys. Res. Lett., 14, 395-398, 1987.

Snyder, A. L., and S.-I. Akasofu, Observations of the auroral oval by the Alaskan meridian chain of stations, J. Geophys. Res., 77, 3419-3430, 1972.

Tholen, S. M., and T. P. Armstrong, Triggering of magnetospheric particle bursts by SSC events, in Solar Wind-Magnetosphere Coupling, ed. by Y. Kamide and J. Slavin, Terra Publishing Co., Tokyo, 1986.

Tighe, W. G., and G. Rostoker, Characteristics of westward travelling surges during magnetospheric substorms, J. Geophys., 50, 51-67, 1981.

Tsyganenko, N. A., and A. V. Usmanov, Determination of the magnetospheric current system parameters and development of experimental geomagnetic field models based on data from IMP and HEOS satellites, Planet. Space Sci., 30, 985-998, 1982.

Ullaland, S. L., K. Wilhelm, J. Kanges and W. Riedler, Electron precipitation associated with a sudden commencement of a geomagnetic storm, J. Atmos. and Terr. Phys., 32, 1545-1553, 1970.

Vorob'yev, V. G., Sc-associated effects in auroras, Geomagn. Aeron., 14, 72-74, 1974.

Wiens, R. G., and G. Rostoker, Characteristics of the development of the westward electrojet during the expansive phase of magnetospheric substorms, J. Geophys. Res., 80, 2109-2128, 1975.

## FIGURE CAPTIONS

Figure 1. The distribution of auroral luminosities over the North American continent at 0241 UT on 8 November 1981 [after Frank et al., 1985]. A coastline map is superposed on this false-color image of the aurora borealis at ultraviolet wavelengths 123-155 nm (filter 2). Principal emissions detected at these wavelengths are from the multiplets of atomic oxygen at about 130.4 and 135.6 nm and from the LBH bands of molecular nitrogen. For the false-color format, luminosities less than about 1 kR are coded black. For greater luminosities the code progresses from red through orange to yellow. Typical luminosities in the sunlit hemisphere are 20-30 kR, with the largest values observed near the subsolar point.

Figure 2. The distribution of auroral luminosities over Antarctica at 0022 UT on 11 May 1983 [after Frank et al., 1985]. A coastline map is superposed on this false-color image of the aurora australis at ultraviolet wavelengths identified in the caption of Figure 1. This image exhibits a theta aurora which comprises the auroral oval and a transpolar arc. The transpolar arc extends into the polar cap from local midnight, traverses the polar cap, and joins with the auroral oval at local noon.

Figure 3. An image of the sunward portion of the northern auroral oval exhibits the gap in discrete aurora which can occur in the local noon sector. The gap is readily detected in the absence of bright diffuse emissions at lower latitudes, which are present in the images of Figures 1 and 2. Three auroral arcs are seen in the evening sector near the lower central part of the image, and bright, active aurora are visible at the lower right as part of the westward boundary of the expanding auroral bulge in a substorm. Contours identifying the Earth's limb and

terminator are overlaid on this image (0154 UT, 8 December 1981). The sunlit hemisphere is observed in the left part of the image. Principal emissions are from the LBH bands of molecular nitrogen.

Figure 4. This unique image of Earth from Dynamics Explorer 1 at 1215 UT on 1 March 1982 records aurora in the two polar regions: The aurora borealis at northern latitudes and aurora australis at southern latitudes. Earth's limb and coastal outlines are overlaid on the image. The spacecraft is located within Earth's umbral shadow cone at an altitude of about 20,000 km above the Pacific Ocean. The active aurora in the two hemispheres rise to altitudes of about 370 km above the limb of the solid Earth. Resonantly scattered solar Lyman-α radiation from Earth's extended hydrogen atmosphere is responsible for the diffuse glow beyond Earth's limb. The dark band encircling Earth above the limb is due to absorption of the ultraviolet radiation by the atmosphere at low altitudes. Passband of the filter for this image extends from 117 - 165 nm.

Figure 5. The $Z_{gsm}$ component of the interplanetary magnetic field at Earth (upper panel) and the auroral electrojet index AE (lower panel) for the 54-hour interval from 0000 UT on 24 October 1981 through 0600 UT on 26 October 1981. The times of nine selected DE auroral images presented in Figure 6 are identified here by the dark vertical bars across the center of the figure.

Figure 6. A series of nine DE auroral images taken in consecutive orbits to illustrate the gross large-scale spatial distribution of the aurora during a time interval in which the interplanetary magnetic field is first oriented northward (images 1-2), southward (images 3-7) and again northward (images 8-9), (see also

Figure 5). Below each image is overlaid the year, day of year and time (UT) of that image. Identification of the filter for each image is provided in Table 1.

Figure 7. Image of the northern auroral oval and polar cap at 0538 (UT) on 25 March 1982 [after Huang et al., 1989]. This image is one of 13 for the time interval 0514 to 0757 UT which exhibit a transpolar arc within the polar cap. Motion of the arc is towards the evening sector during a period in which the IMF $B_y$ component is positive.

Figure 8. A position on the transpolar arc of 25 March 1982 (Figure 7) mapped to $X_{gsm} = -12\ R_e$ in order to summarize its motion. The position is approximately equidistant between the two intersection points of the arc and the auroral oval. The magnetic field model of Tsyganenko and Usmanov [1982] is used. Average speed as determined by a least-squares fit to the data is 6.6 km/s, and the motion is in the direction of the IMF $B_y$ component, which is positive.

Figure 9. A continuation of Figure 8 for the transpolar arc of 10-11 May 1983 observed in the southern hemisphere (see also Figure 2). Average speed is 8.9 km/s in the direction opposite to the direction of the IMF $B_y$ component, which is positive.

Figure 10. Hourly averages of $D_{st}$ and the three-hour values of $K_p$ for 20-22 October 1981. Onset times are identified for two geomagnetic storm sudden commencements (SC). The direction of the arrow for each SC specifies whether the IMF is oriented southward (down) or northward (up).

Figure 11. Sequence of 12 consecutive false-color auroral images at ultraviolet wavelengths in the time interval 0417 - 0650 UT on 22 October 1981 [after Craven et al., 1986]. Increasing luminosities follow the SC at 0525 UT (beginning of the sixth frame). Predominant direction of the IMF $B_Z$ component is northward. Below each image is the year, day of year and time (UT) for the beginning of the 12-min telemetry period for the image.

Figure 12. (a) Maximum luminosities of ultraviolet emissions along the auroral oval in the noon, dusk and midnight sectors for the two-hour interval surrounding the SC at 1309 UT on 20 October 1981 (images not shown). (b) Continuation for 22 October 1981 and the SC at 0525 UT (images shown in Figure 11). Averages are given for the intensities in the dawn and dusk sectors.

Figure 13. A sequence of 16 images of the aurora australis in the time interval 0202 - 0517 UT on 13 June 1983 [after Frank and Craven, 1988]. Intense auroral activity begins in the first image at upper left with a localized brightening (substorm onset) followed by a period of rapid expansion of the aurora in latitude and in longitude. Luminosities increase noticeably by 0326 UT (eighth image), indicating the arrival at Earth of a shock or discontinuity in the interplanetary medium. This auroral activity occurs simultaneously with the main phase decrease of the low-latitude surface magnetic field during a geomagnetic storm.

Figure 14. Histogram which shows the number of substorm onsets in half-hour increments of magnetic local time (MLT) along the auroral oval from a set of 68 well-defined substorm onsets identified with DE 1.

Figure 15. Hourly averages of the $D_{st}$ index for the 15-day interval from 6-20 June 1983. The sudden commencement (SC) is at 0118 UT. The images shown in Figure 13 are from the time interval of the main phase decrease.

Figure 16. Latitudinal motions of the aurora for the imaging sequence presented in Figure 13 and the auroral activity index AE for the time interval 0100 - 0600 UT. The equatorward and poleward boundaries of the aurora are presented in the upper panel for the three magnetic local times 2000, 2200 and 2400 MLT, and in the center panel for 0000, 0200 and 0400 MLT. The contours for local midnight are reproduced in both panels to assist in evaluating the variations with local time. No sharp increase exists in the AE index that clearly is associated with the luminosity enhancement at about 0202 UT, but the index is increasing at that time.

Figure 17. Four auroral images selected to illustrate variations in the longitudinal distribution of aurora which can be observed during the expansion phase of substorms. The first image, at upper left, features an expansion which does not proceed westward of 2200 MLT (the surge is nearly stationary) and the auroral bulge expands predominantly into the morning sector. The second image, at upper right, shows an auroral bulge more symmetric about the noon-midnight plane and a surge which advances farther into the evening sector. The auroral distribution in the third image, at lower left, is nearly a mirror image of the first image, with the expansion into the evening sector and nearly no eastward expansion into the morning sector. The last image is an example for which auroral activity expands westward rapidly along the auroral oval and there is almost no signature at midnight of an auroral bulge. For this false-color format luminosities less than

about 1 kR are coded black. For greater luminosities the code progresses from blue through green, yellow and red to a saturation value near 20 kR coded white.

Figure 18. Four examples of poleward motion during the expansion phase of a auroral substorm to illustrate observed local time variations.

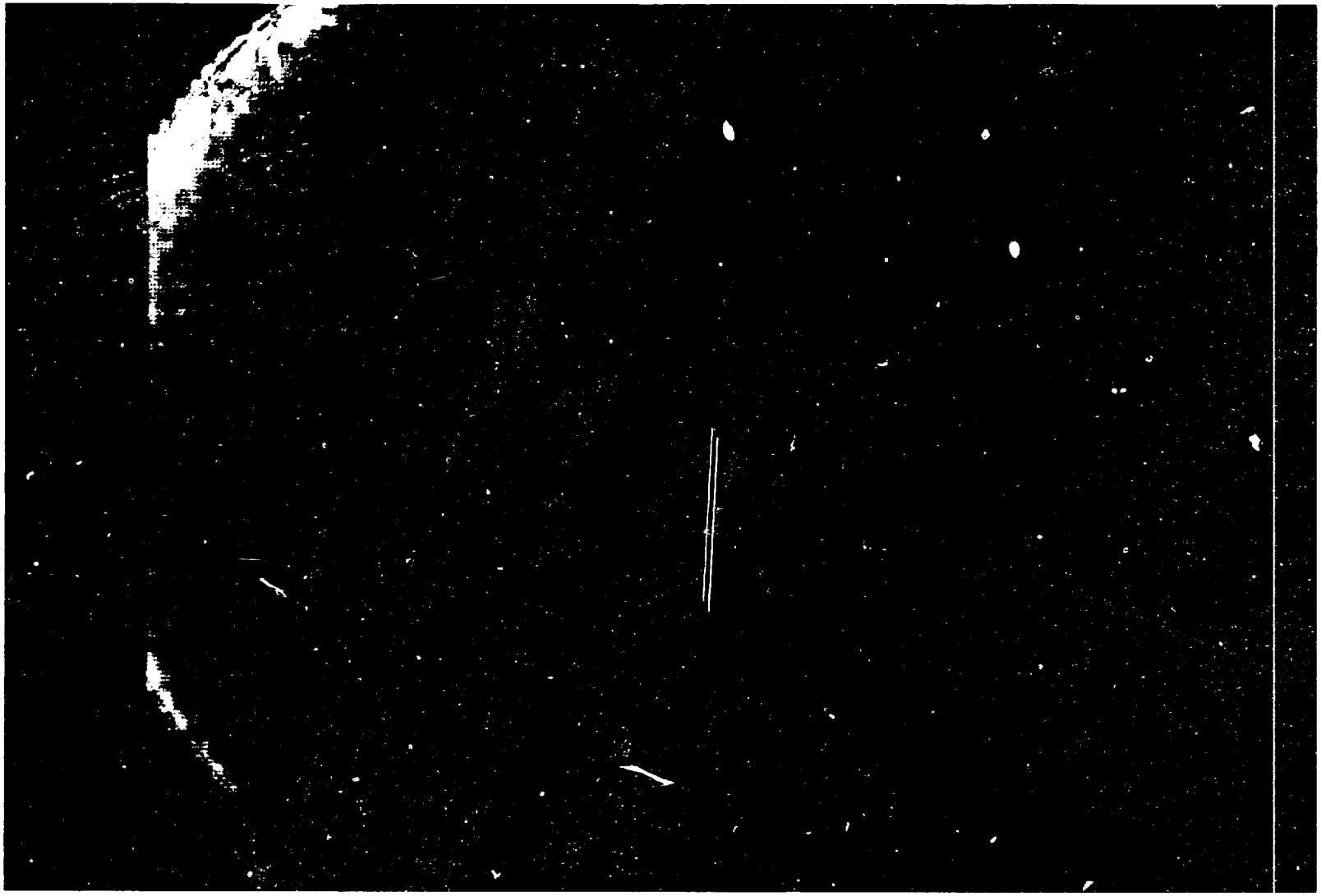

Figure 1

Figure 2

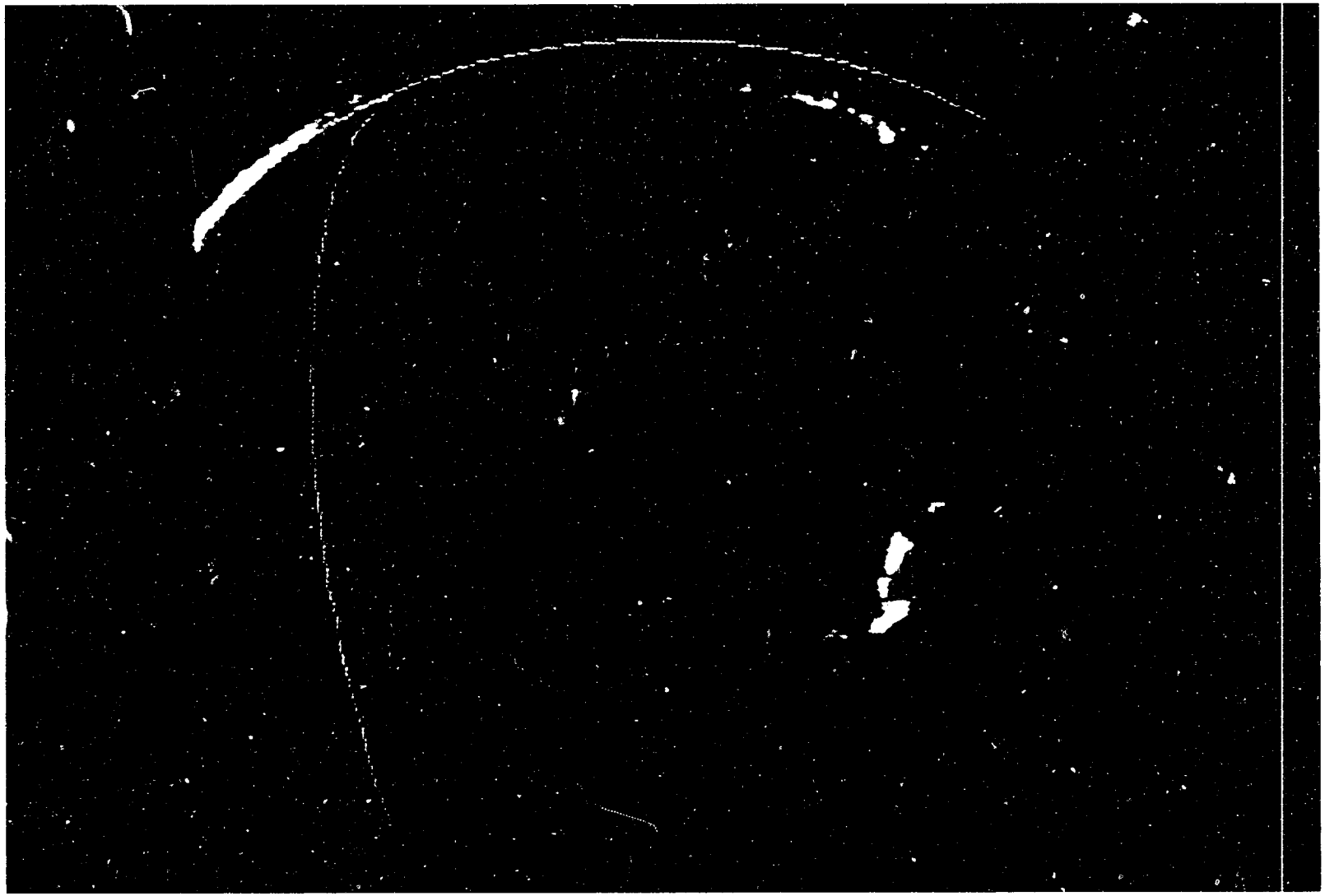

Figure 3

Figure 4

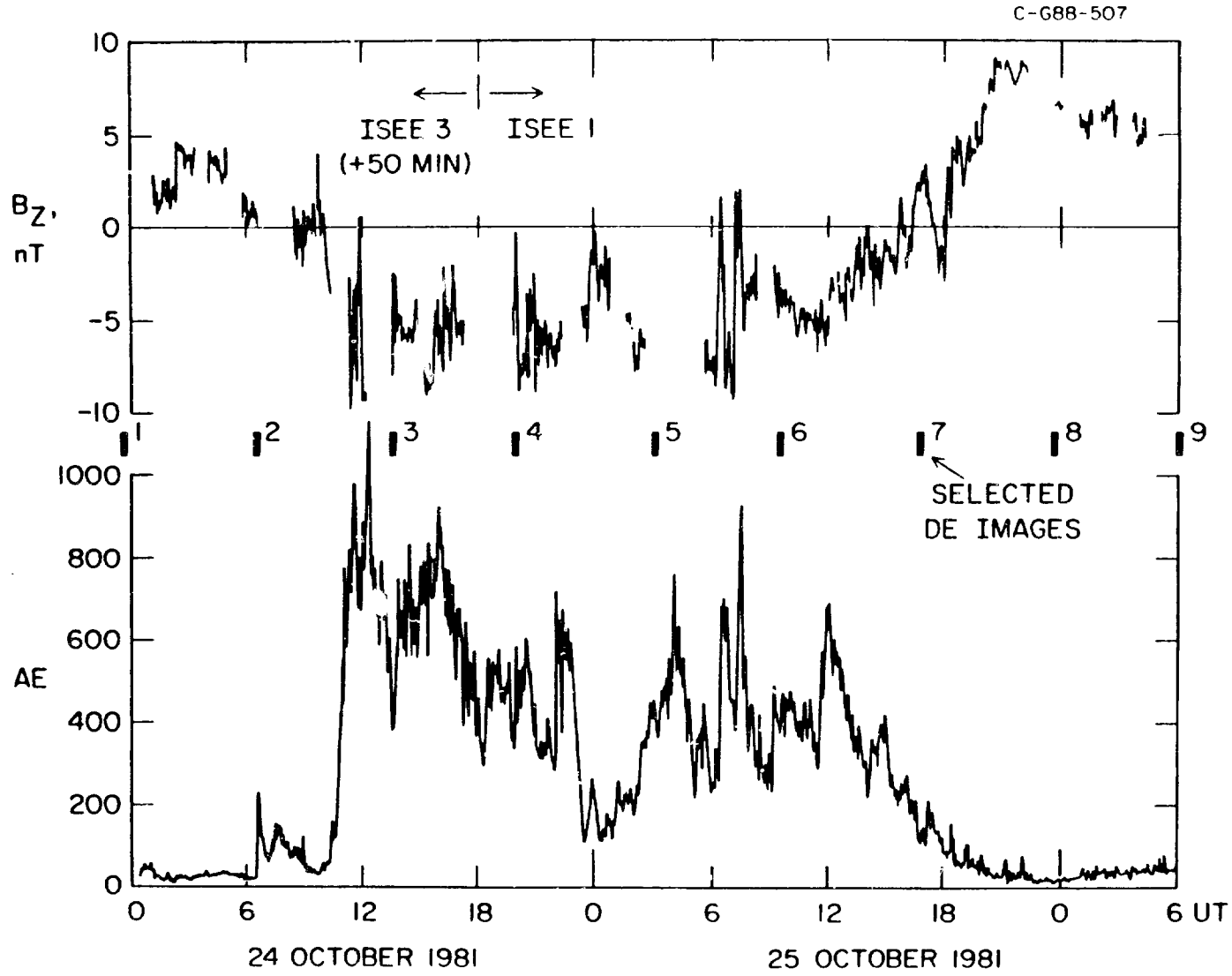
C-G88-507
10
5
0
-5
-10
$B_Z$, nT
ISEE 3
(+50 MIN)
ISEE 1
1
2
3
4
5
6
7
8
9
SELECTED
DE IMAGES
1000
800
600
400
200
0
AE
0
6
12
18
0
6
12
18
0
6 UT
24 OCTOBER 1981
25 OCTOBER 1981

Figure 5

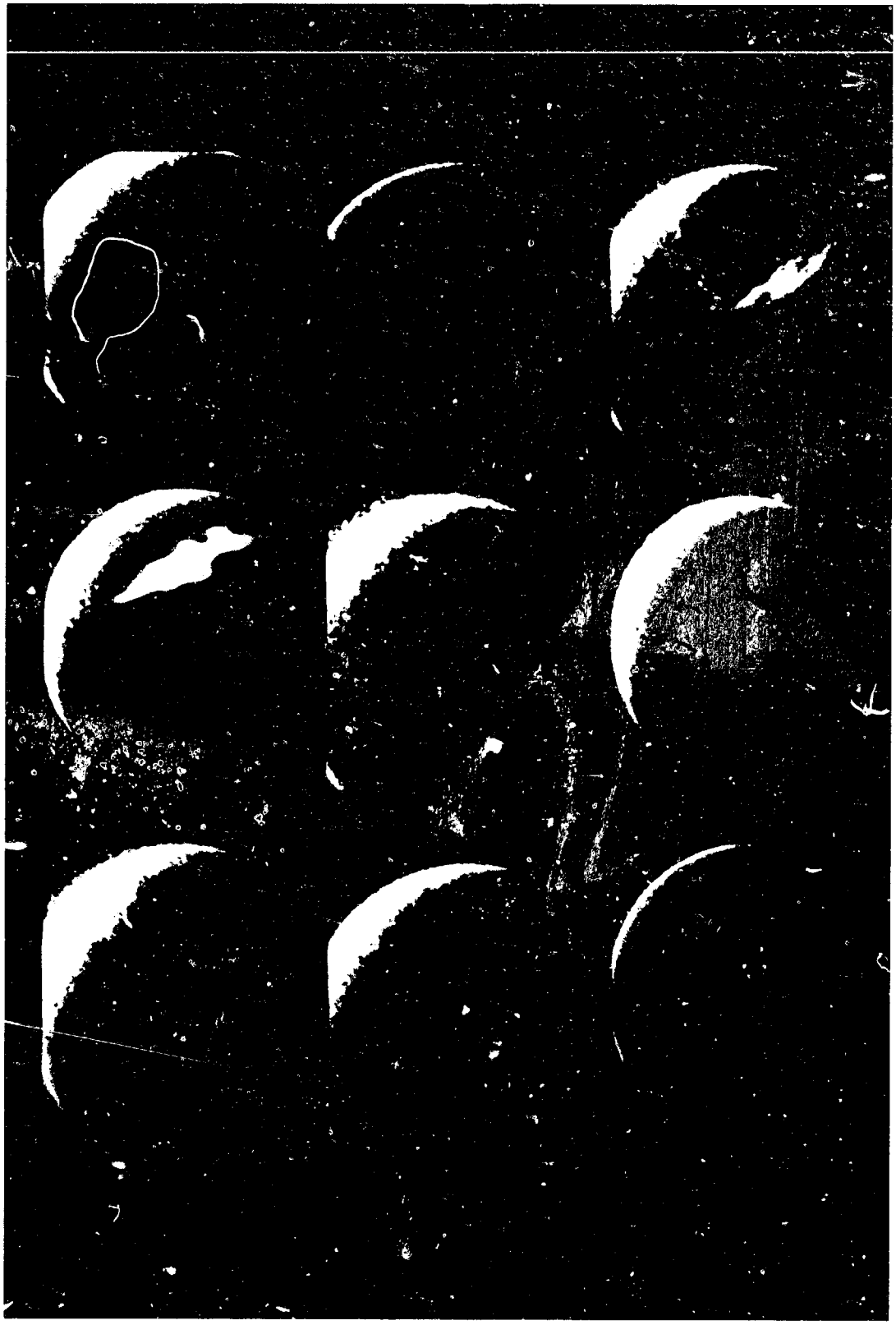

Figure 6

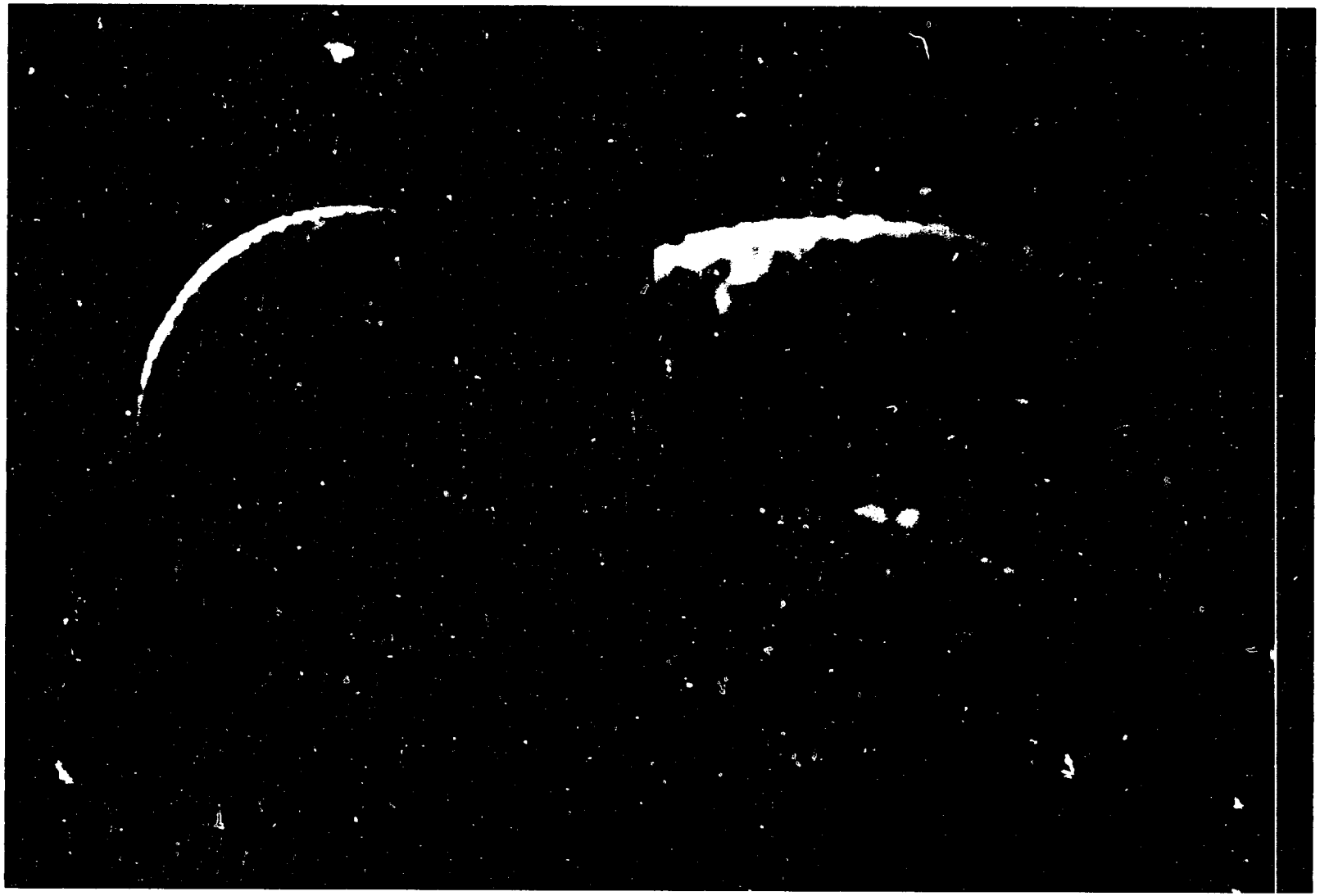

Figure 7

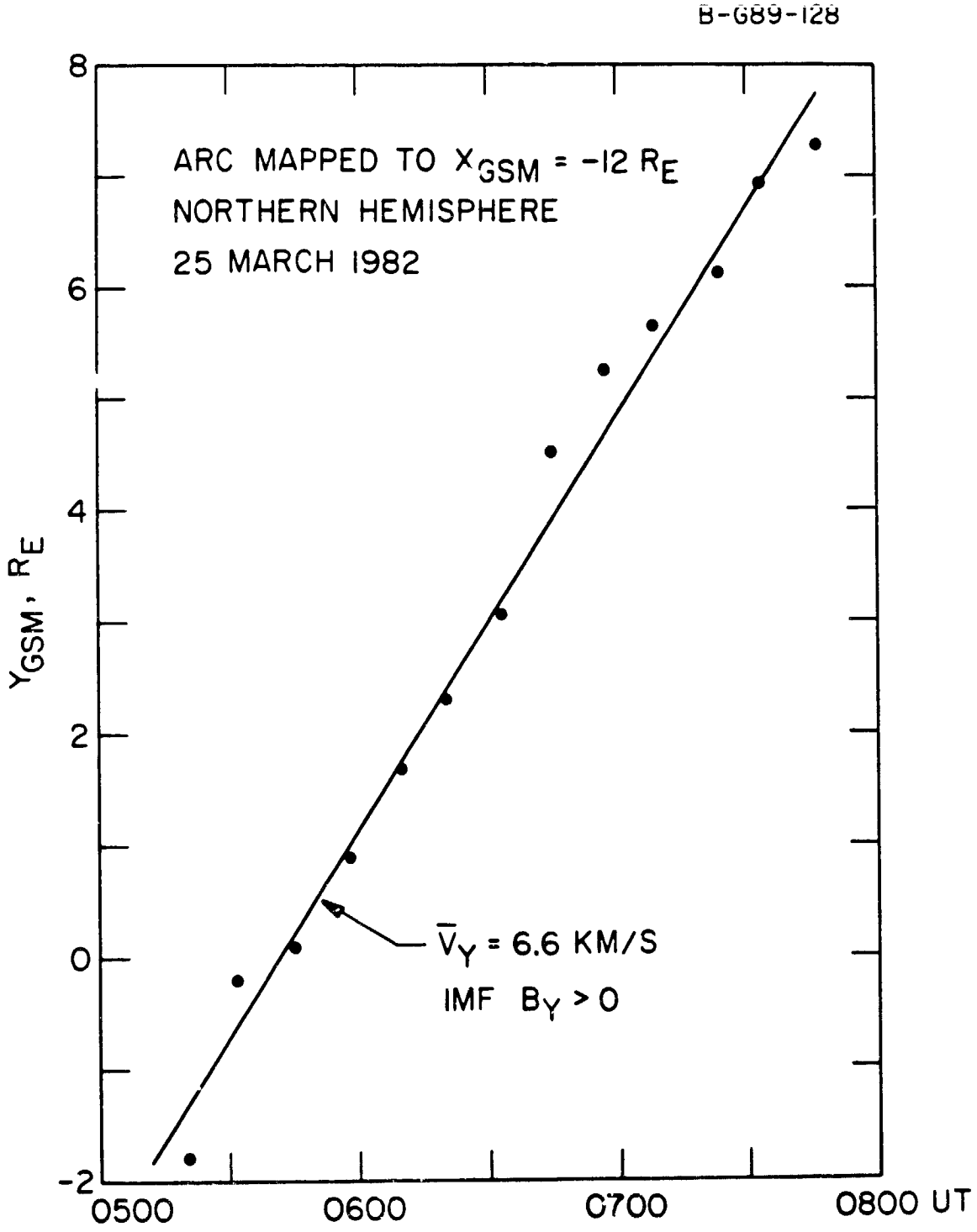
B-G89-128
ARC MAPPED TO $X_{GSM}$ = -12 $R_E$
NORTHERN HEMISPHERE
25 MARCH 1982
$\bar{V}_Y$ = 6.6 KM/S
IMF $B_Y$ > 0
$Y_{GSM}$, $R_E$
8
6
4
2
0
-2
0500
0600
0700
0800 UT

Figure 8

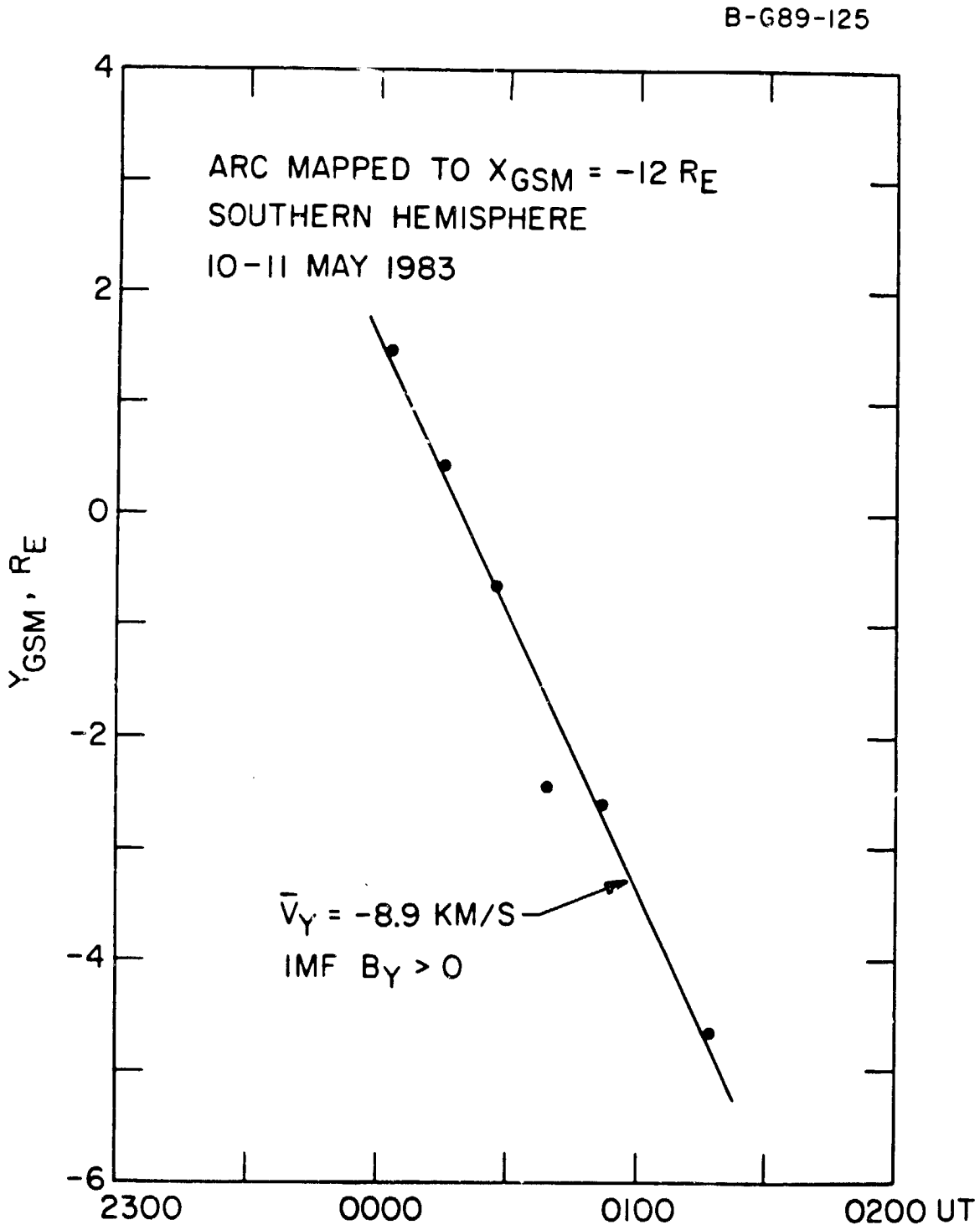
B-G89-125
ARC MAPPED TO $X_{GSM} = -12\ R_E$
SOUTHERN HEMISPHERE
10-11 MAY 1983
$\bar{V}_Y = -8.9$ KM/S
IMF $B_Y > 0$
$Y_{GSM}$, $R_E$
4
2
0
-2
-4
-6
2300
0000
0100
0200 UT

Figure 9

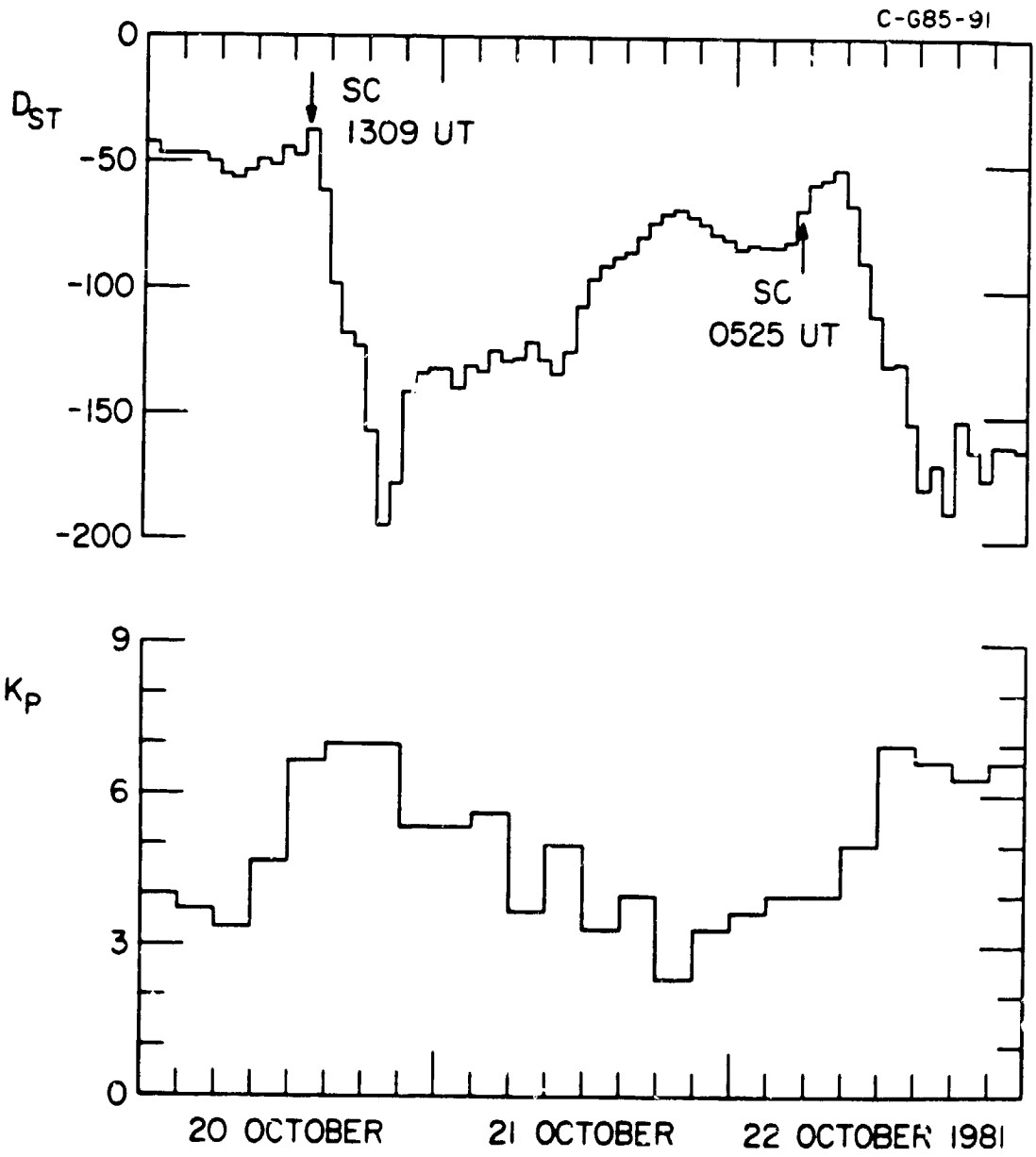
C-G85-91
0
-50
-100
-150
-200
$D_{ST}$
SC
1309 UT
SC
0525 UT
9
6
3
0
$K_P$
20 OCTOBER
21 OCTOBER
22 OCTOBER 1981

Figure 10

Figure 11

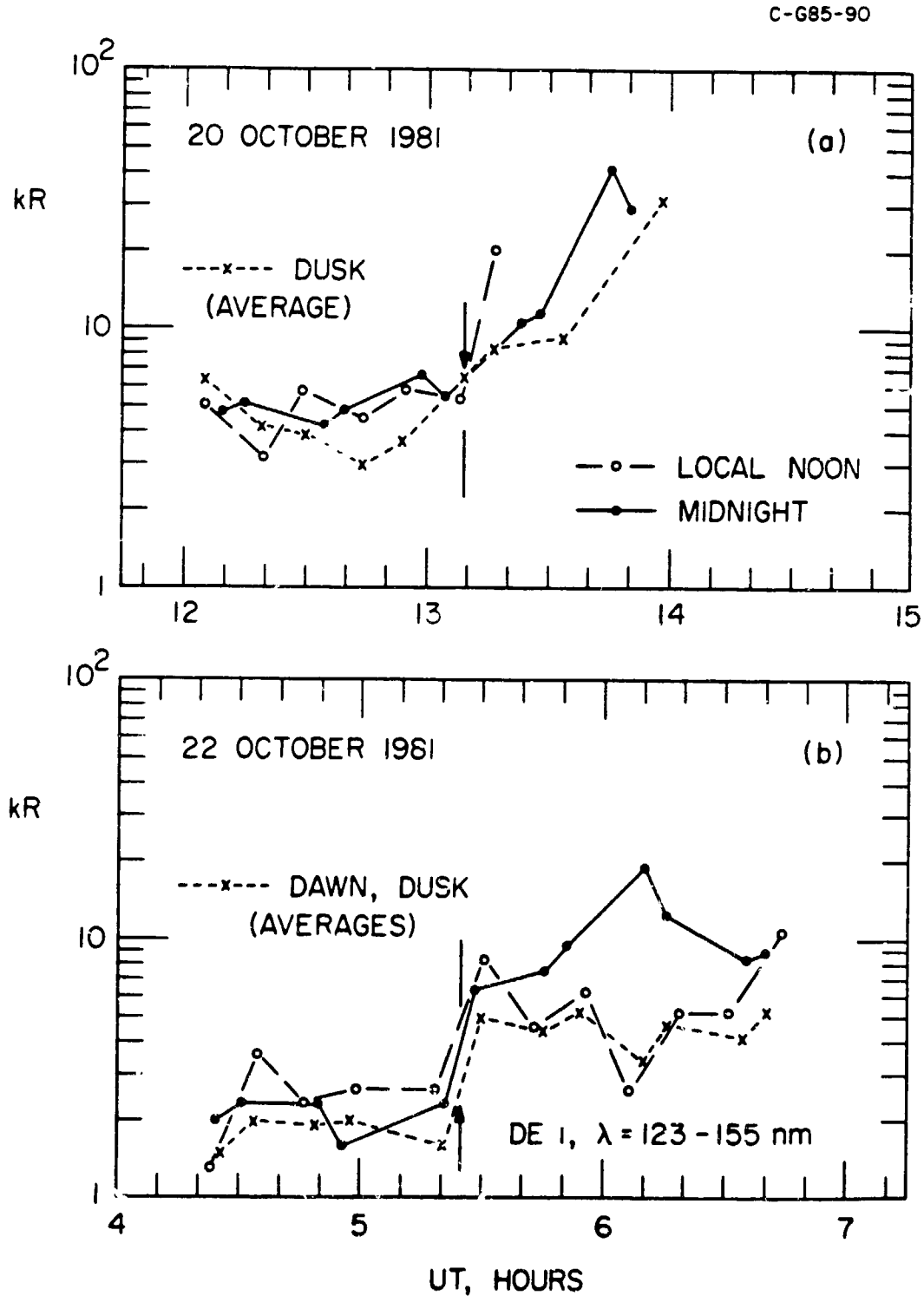
C-G85-90
$10^2$
20 OCTOBER 1981
(a)
kR
---x--- DUSK
(AVERAGE)
10
—o— LOCAL NOON
MIDNIGHT
1
12
13
14
15
$10^2$
22 OCTOBER 1981
(b)
kR
---x--- DAWN, DUSK
(AVERAGES)
10
DE 1, λ = 123 - 155 nm
1
4
5
6
7
UT, HOURS

Figure 12

Figure 13

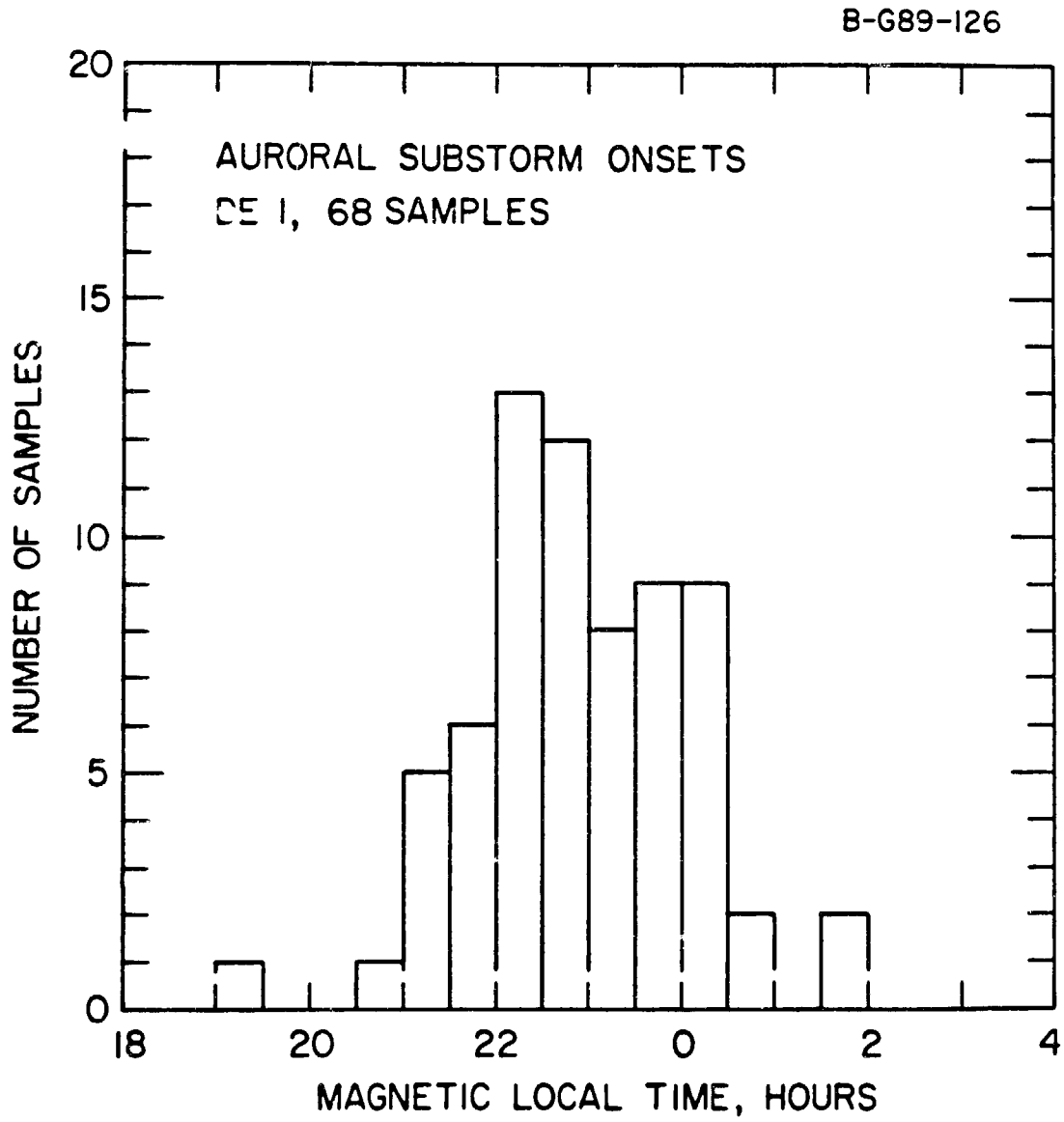
B-G89-126
AURORAL SUBSTORM ONSETS
DE 1, 68 SAMPLES
NUMBER OF SAMPLES
0
5
10
15
20
18
20
22
0
2
4
MAGNETIC LOCAL TIME, HOURS

Figure 14

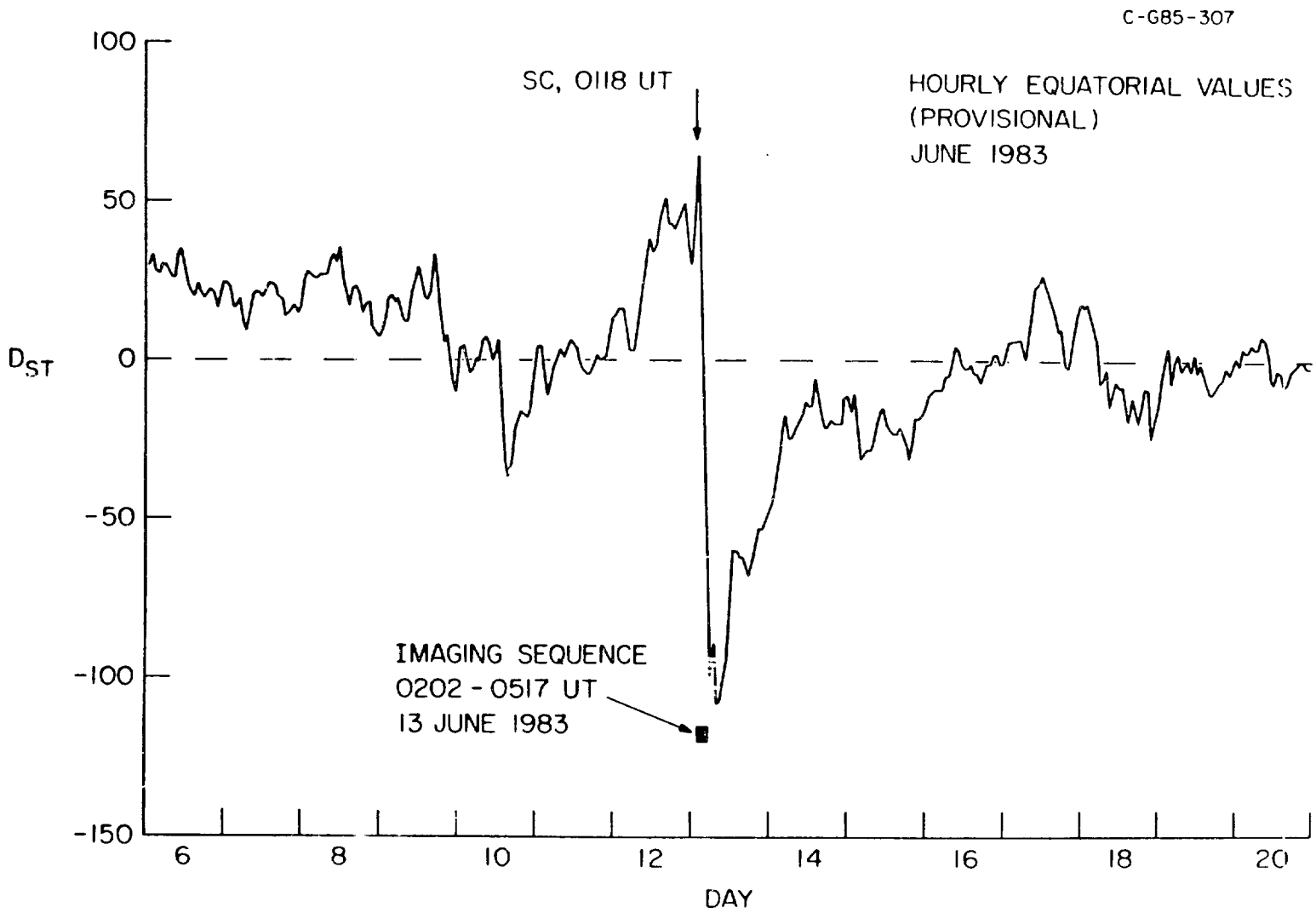
C-G85-307
SC, 0118 UT
HOURLY EQUATORIAL VALUES
(PROVISIONAL)
JUNE 1983
100
50
0
-50
-100
-150
$D_{ST}$
IMAGING SEQUENCE
0202 - 0517 UT
13 JUNE 1983
6
8
10
12
14
16
18
20
DAY

Figure 15

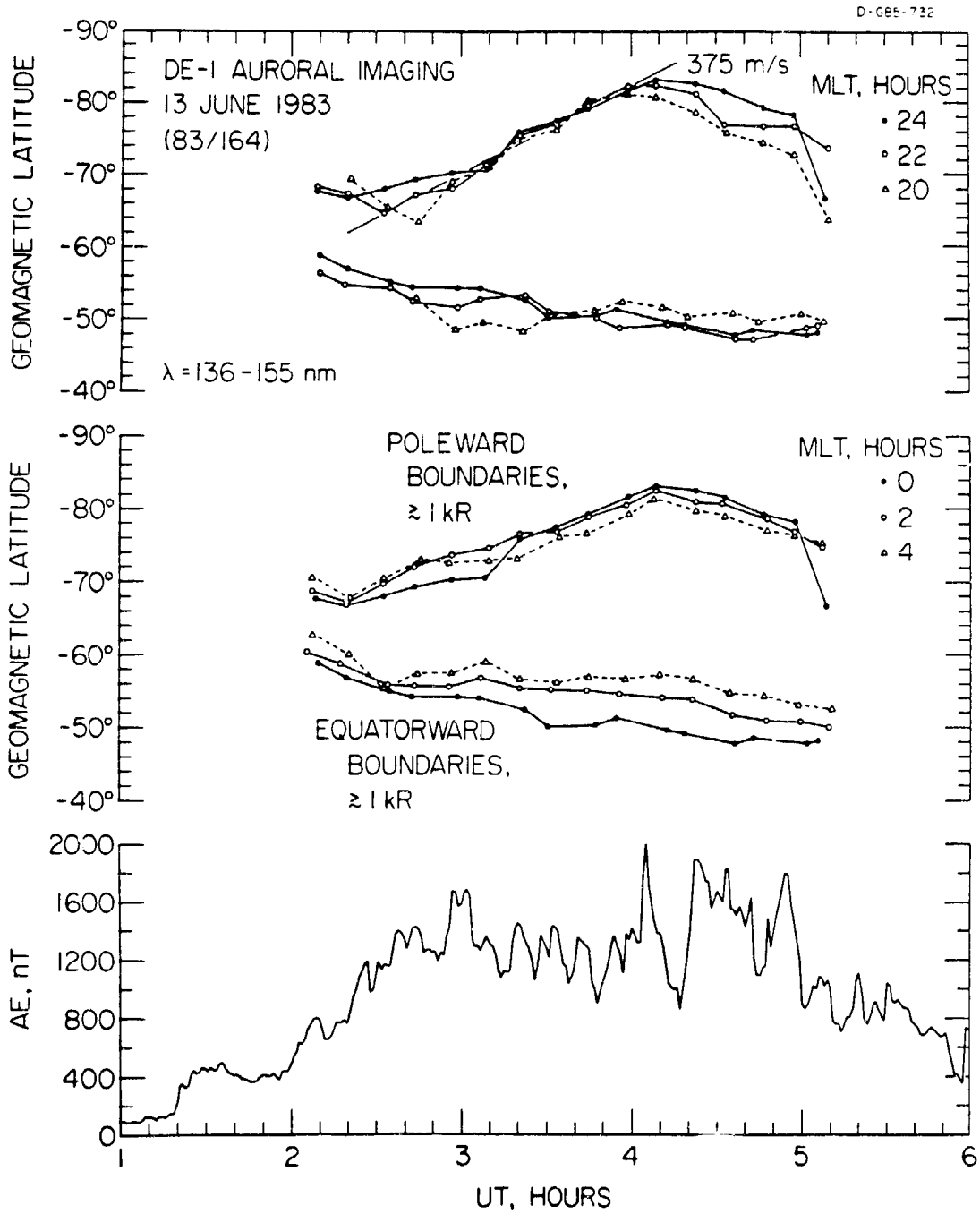
D-GBS-732
DE-1 AURORAL IMAGING
13 JUNE 1983
(83/164)
λ = 136 - 155 nm
375 m/s
MLT, HOURS
• 24
◦ 22
▵ 20
GEOMAGNETIC LATITUDE
-90°
-80°
-70°
-60°
-50°
-40°
POLEWARD
BOUNDARIES,
≳ 1 kR
EQUATORWARD
BOUNDARIES,
≳ 1 kR
MLT, HOURS
• 0
◦ 2
▵ 4
AE, nT
2000
1600
1200
800
400
0
1
2
3
4
5
6
UT, HOURS

**Figure 16**

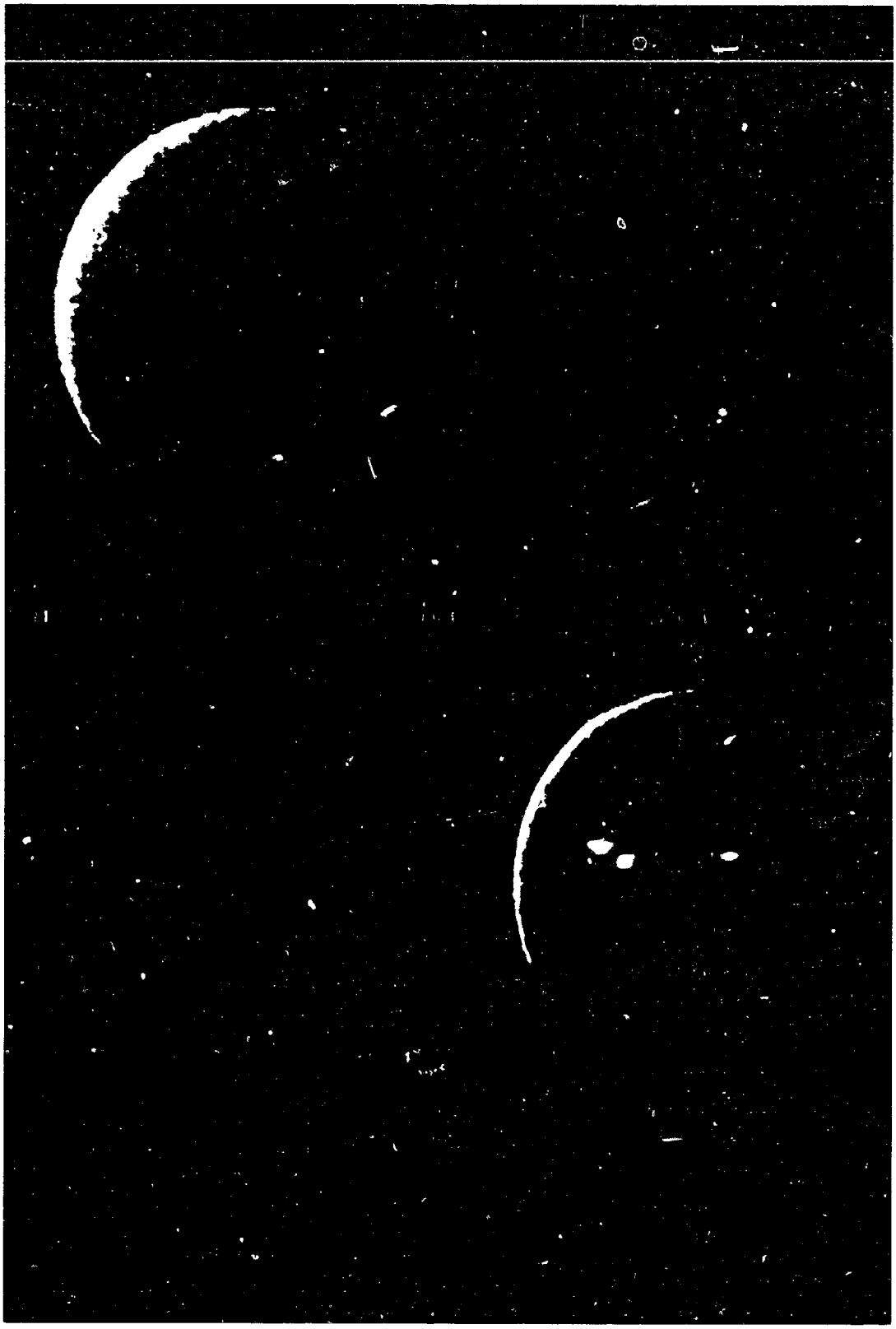

Figure 17

ILLUSTRATIVE EXAMPLES —

POLEWARD EXPANSION OF THE AURORA IN SUBSTORMS

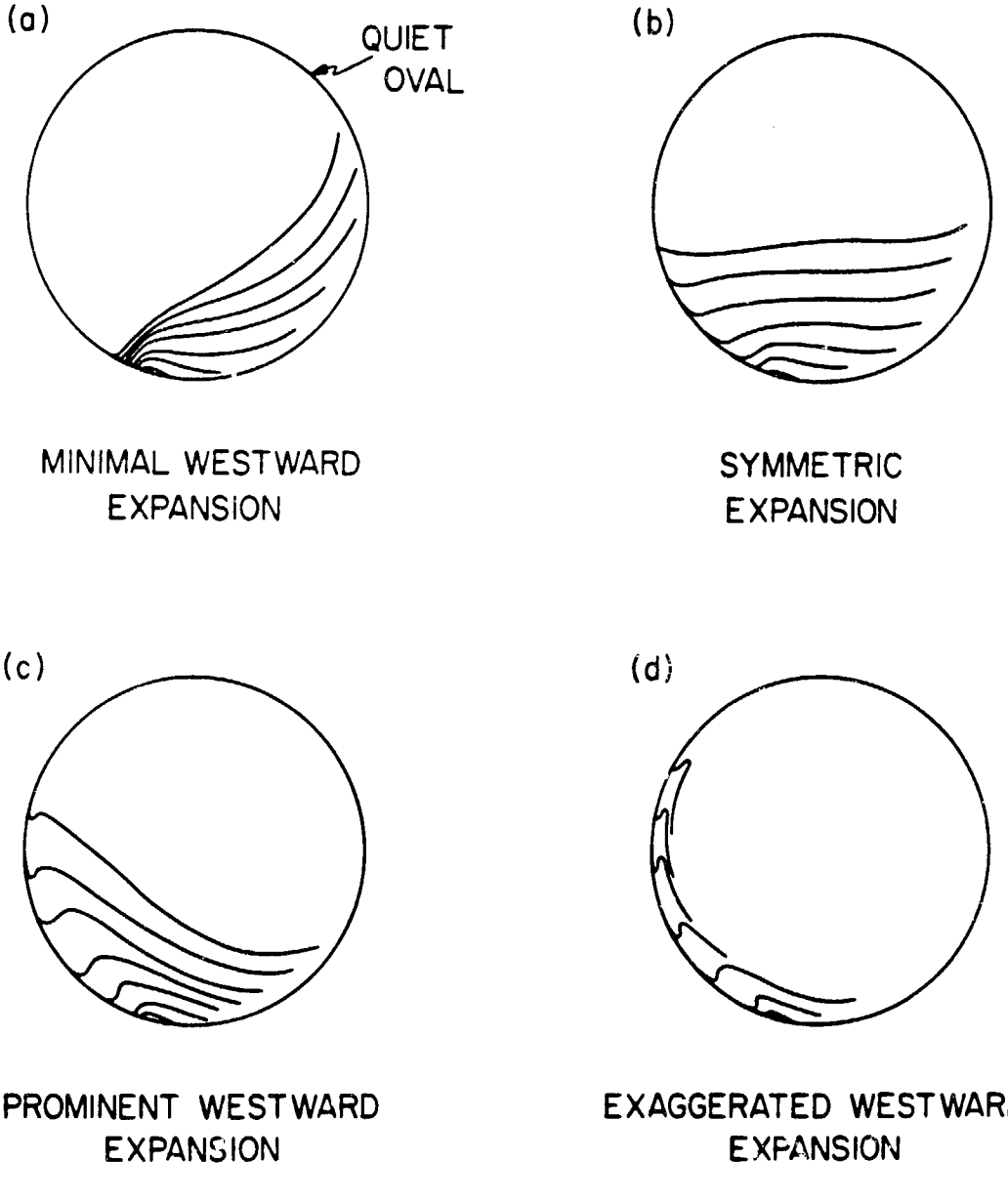


Figure 18